Internal Hydraulics, Solitons and Associated Mixing in a Stratified Sound

by

Jianping Gan

A thesis submitted to the Faculty of Graduate Studies and Research, McGill University, in partial fulfilment of the requirement for the degree of Master of Science

Department of Meteorology
McGill University
Montreal, Quebec
Canada, H3A 2K6

December, 1990

ABSTRACT

Observations of tidally forced flow in a constricted region of a highly stratified sound are examined as a problem of two-layer hydraulic exchange. It is shown that the narrowest section and the region downstream of the narrowest section were subject to internal hydraulic control. The internal bores are generated downstream of the control section during the flood, when flow transits between subcritical and supercritical flow. The shoaling region near a small island might generate the critical and supercritical flow, and hence an internal drop during the ebb. Bores moved upstream and evolved into packets of internal solitary waves with 3-6 minute period when the tide turned to ebb. Solitary wave properties are reviewed. Combined with the results of hydraulic control in the sound, a generation mechanism for solitary wave is then considered. Using results from different models of the solitary wave based on the KdV equation, it is shown that the second-order nonlinear term must be included in the two-layer model. The results from a first-order continuously stratified model, solved using the lowest mode eigenfunction, gave similar good results as the second order two-layer model. This implies that two-layer models may ignore some properties of the real fluid and that the internal solitons are also sensitive to the stratification characteristics of the water column. Several possible mixing mechanisms are investigated. It is found that the mixing was related to both the vertical velocity shear, the hydraulic characteristics of the flow and the presence of solitary waves. Dissipation of solitary waves and bores can transfer energy and increase the potential energy of the fluid when they propagate upstream in the sound.

RESUME

Des observations de courants forcés par la marée dans la partie étroite d'un détroit hautement stratifié sont examinées dans le cadre d'un échange hydraulique à deux couches. 11 est démontre que la partie la plus étroite et l'aval de cette partie sont sujet à un contrôle hydraulique interne. Les mascarets internes reliés se produisent lorsque le courant passe de sous-critique à super- critique en aval de la région de contrôle durant la marée montante. La zone moins profonde près de la pente d'une petite ile pourrait générer un courant critique et super-critique, et donc un mascaret durant la marée descendante. Les mascarets se déplacent vers l'amont et deviennent des paquets d'ondes solitaires internes ayant une période de 3 a 7.5 minutes quand la marée commencée à se retirer. Les propriétés des ondes solitaires sont passées en revue. En combinant celles- ci avec les résultats du contrôle hydraulique dans le détroit, nous proposons un mécanisme d'excitation de ces ondes. Utilisant des résultats de différents modèles d'ondes solitaires basés sur l'équation KdV, nous démontrons que le terme non- linéaire d'ordre deux doit être inclus dans le modèle à deux couches. Par contre, les résultats du modèle d'ordre un avec une stratification continue, résolu pour la fonction d'état du premier mode, étaient aussi bons que les résultats obtenus avec le modèle d'ordre deux à deux couches. Ceci implique premièrement que le modèle à deux couches ne tient pas compte de certaines propriétés des fluides réels et deuxièmement que les solitons sont sensibles aux caractéristiques de la stratification de la colonne d'eau. Plusieurs mécanismes possibles de mélange sont examinés. Nous avons constaté que le mélange est relié aux caractéristiques hydrauliques du courant. La dissipation des ondes solitaires et des mascarets internes peut transférer de l'énergie et augmenter l'énergie potentielle du fluide lorsqu'ils se propagent vers l'amont du détroit.

ACKNOWLEDGEMENTS

The author wishes to thank Claud Belanger and Paul Peltola for their efforts in collecting and processing the original data, Tincke Van der Baaren for her assistance in the English editing of this manuscript, Professor D. M. Farmer, T. Warn and Dr. J. Sheng for helpful discussions. In particular, I would like to thank my thesis director, Professor R.G Ingram, for his helpful suggestions and constant encouragement during my studies.

In addition, special thanks go to Ursula Seidenfuss for drafting the figures and Paul Vaillancourt for translating the Abstract.

This work was partially supported by the Groupe Interuniversitaire de Recerche Oceanographiques du Quebec.

CONTENTS

LIST OF TABLES

LIST OF FIGURES

Chapter 1.Introduction:

Many observations and theoretical studies have shown that the interaction of a stratified flow with a sill and/or constriction will alter the flow in many ways. Both sill and constriction can act as a hydraulic control whenever the internal Froude number (defined subsequently) reaches a critical value. The control region separates subcritical flow upstream from supercritical flow downstream and its location is a function of the width, depth and stratification in a channel. The occurrence of the internal hydraulic bore in the two-layer flow is related to the transition between the subcritical flow and the supercritical region downstream of the control.

In a stratified ocean, the initial disturbance of the density interface (internal lee wave,jump or bore, etc), which arises from the interaction between tidal current and topography and/or constriction, can be very nonlinear. It may result in an internal solitary wave (a wave which retains shape and phase speed while colliding with each other, also called soliton) with the front of depression or elevation apparently steepening due to nonlinear effects. Based on observations and existing theories, the mechanism of generating internal solitons has been discussed by many authors. (e.g.Maxworthy (1979) and Farmer and Smith (1982)).

Further discussion about the hydraulics in a constricted region with a sill, solitary wave characteristics and applicable theories in the ocean will be presented in chapter 3 and 4.

The strong vertical velocity shear, the hydraulic characteristics of the flow, and the dissipation of the internal hydraulic bore and solitary waves in our study region lead to changes in the salinity structure of our study region. Previous work, such as Partch and Smith (1978), and Lewis (1985) have indicated that intense mixing events were initiated when the internal Froude

number (the ratio of the mean flow to internal long wave speed) reached a critical value. Their results also indicated that the breaking of long internal waves are unable to propagate upstream against the opposing current, and could produce a critical state. Sandstrom and Elliott (1984) found that the dissipation of solitary waves associated with a shoreward propagating internal tide could provide energy for vertical mixing. Both Partch and Smith (1978) and Gardner and Smith (1978) showed that an internal jump itself might generate mixing without the presence of internal waves and might be responsible for the intense mixing.

Data from previous studies (Legendre et al,1981, Ingram, 1983) have shown the progressive thinning of the pycnocline and an increase in salinity of the upper layer with distance into highly stratified Manitounuk Sound (southern Hudson Bay, fig.1.1). Further details about conditions in the sound can be found in Ingram (1981; 1983). In particular, Ingram suggested that one of the sources of denser water for the upper layer was vertical exchange near Paint Islands (fig.1.1). A hydraulic mechanism which may increase vertical exchange was recently suggested by Ingram et al (1989). They assumed that the breaking of high frequency internal waves, generated at a constriction, could cause upward salt transport across the pycnocline However, their observations were taken every 5 minutes, resulting in an aliasing of the high frequency fluctuations of 3-5 min. period.

The object of this thesis is to gain insight into the importance of internal solitons and their effect on mixing based on the analysis of hydraulic characteristics in a constricted sound. Following a brief review of the theory on internal hydraulics and applications in Chapter 3, a two-layer internal hydraulic exchange model is used to determine the possible existence of hydraulic controls over a tidal cycle. Both the location of these controls and the way in which they influence the dynamics in the sound are

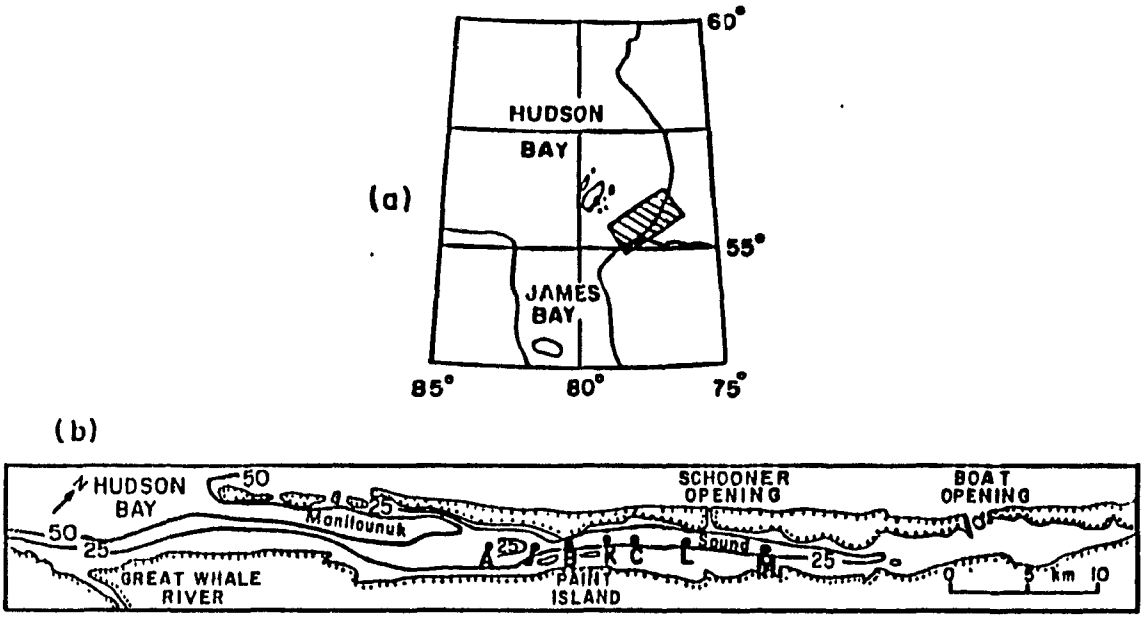

Figure 1.1. Local bathymetry and station location in Manitounuk Sound

considered. Based on the current and salinity data, it will be shown that when the flood in the upper layer reached a maximum, flow became critical at the constriction, and a hydraulic bore was formed downstream. Analysis of the results also indicated other control sites might exist near both the downstream of the narrowest section and the shallow region near a small island in the sound. Supercritical conditions at this time occurred downstream of these controls, which may account for the generation of the strong upper layer bore and drop. The bore and drop in this thesis are defined as a sudden upward (ridge) and downward (trough) steepening of the crest. This study of the hydraulics in the sound will also help us to understand the configuration of the pycnocline structure along the sound during the observation period.

Spatial and temporal characteristics of the high frequency internal waves generated during the measurement period are considered on the basis of hydraulics and nonlinear wave theory in Chapter 4. By using the solutions of the Korteweg-de Vries (KdV) equations, both for two-layer and continuous stratification models, the parameter values of the wave and their comparison with observations are given. The model experiment shows that the second order correction in the two-layer model seems necessary, but that the first-order approximation is adequate for continuous stratified conditions.

After discussing the mechanisms of the internal hydraulics and high frequency waves, the high mixing rate in the sound is considered. In Chapter 5, it will be shown that when the composite Froude number exceeded a critical value, the flow became more unstable in the sound. The instability is described as a Kelvin-Helmholtz shear instability. Subsequent dissipation of the solitary waves and bores transferred their energy to create increased mixing in the sound.

Chapter 2.Observations

Manitounuk Sound is a 60km long coastal embayment in southern Hudson Bay aligned in a NE direction (fig.1.1). Depth varies from 70-90m near its entrance to less than 10m near the inland termination. The average width in the sound is about 3km with a horizontally constricted region of about 1.5km wide near Paint Islands. Two inlets inside the sound, Schooner and Boat Openings, connect it with Hudson Bay. However, the water exchange through both openings is minor and their effects can be ignored (Ingram et al, 1989). A small island is located about 5km upstream of the constricted region. In general, the sea ice cover is of the landfast type and forms in early December and breaks up in late June. The average ice thickness is about 1- 1.5m. At the entrance of the sound, the Great Whale River provides the only major fresh water source. Due to the intrusion of brackish water associated with the plume of the river and ice melt in spring, the sound can be characterized as highly stratified from mid-winter to early summer.

Previous observations in south-east Hudson Bay and Manitounuk Sound were made in 1982-83 (Larouche, 1984). His data showed that the salinity and temperature in the upper layer of the pycnocline gradually increased offshore from the exit of the Great Whale River into Hudson Bay. CTD data in the sound indicated that the strongest stratification was located near the entrance and decreased inward. A 24 hour continuous series of CTD profiles, in the constricted region of the sound, taken just two days after maximal spring tide, revealed that the typical pycnocline depth was about 2-3m beneath the ice cover. However, since their sampling interval was 30 min, higher frequency signals were not observed.

Our project was designed to study the hydraulics and high frequency waves generated in the sound. Analysis in this thesis will be based on salinity, temperature and current data observed in the sound during spring tide.

Current meters were moored at stations A, B and C (figs.1.1 and 2.1).

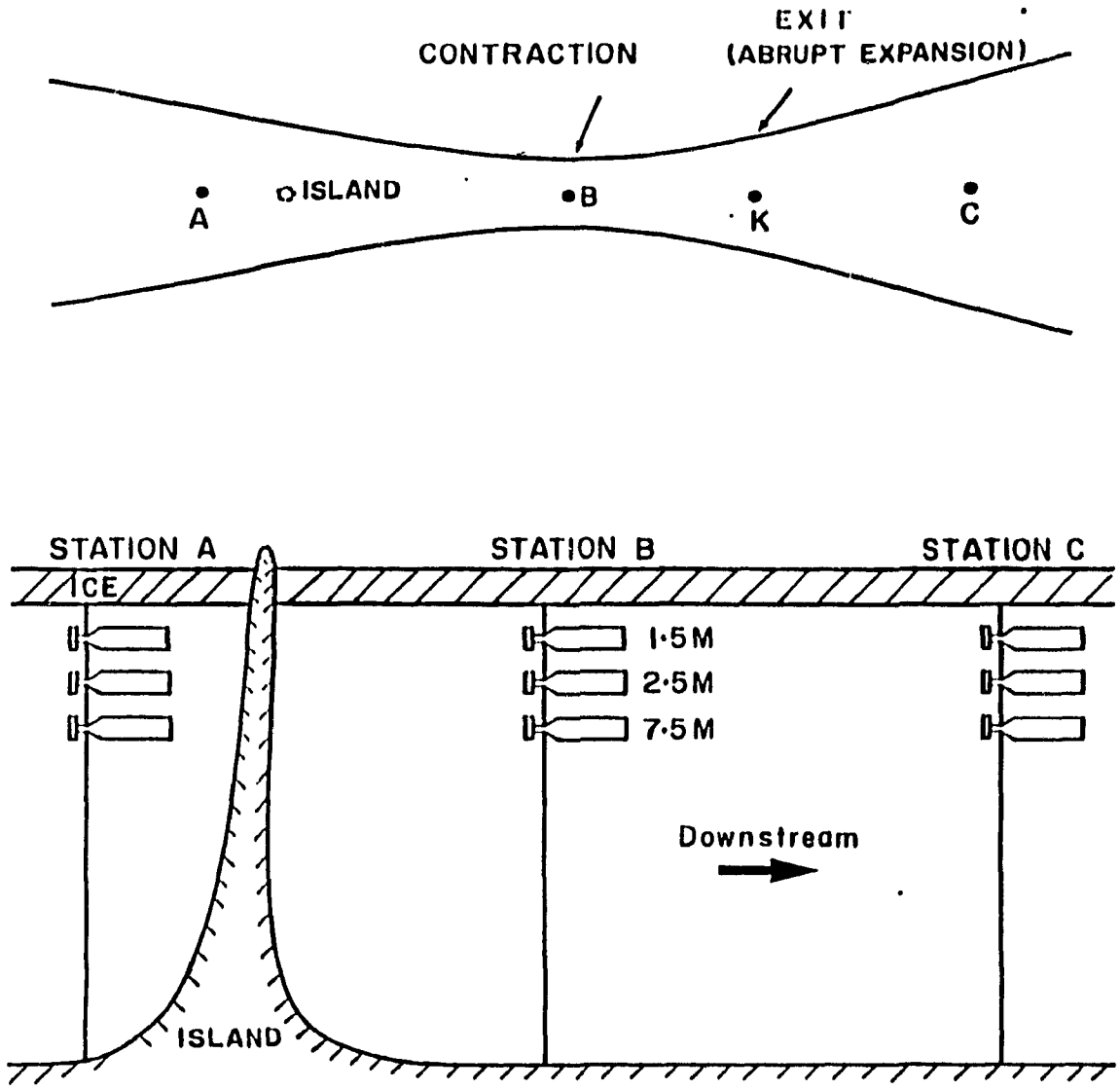

Figure 2.1 Current meter mooring location

The distance between the individual stations was 5.2km, with station A behind a small island, B at the narrowest section, and C downstream of the constriction. At each station, Aanderaa current meters (RCM4 or RCM7) were moored at depths of 1.5, 2.5 and 7.5m below the underside of the ice, and sampled velocity, temperature and conductivity every minute. The accuracy of the recording current meter (both RCM 4 and RCM 7) is ±0.05 ^{0}C, ±0.025 mmho/cm and ± 1cm/sec for temperature, conductivity and velocity, respectively. The recordings of temperature, conductivity and pressure was instantaneous. However, the velocity value was based on averaging during the 1 min sampling interval for RCM4 and on vector averaging every 12 s for the RCM7. CTD (conductivity, temperature, and depth) profiles were also taken at stations A,J,B,K,C,L, and M (fig.2.2). The observations took place April 14 to May 2,1989. The predicted average tide amplitude was about 2m during the observation period, with the maximal tide of 3.5m occurring during the spring tide of 23 April (fig.2.3).

Our CTD profiles showed relatively strong stratification in the sound. The pycnocline was located at about 2.5-3.0m beneath the ice cover. Below the pycnocline, the salinity increased smoothly with depth. Similar to the previous study by Ingram (1983), a gradual increase of near-surface salinity from stations A to M could be seen, with the largest near-surface increase from stations B to C. The stratification was the strongest at stations A to K and the weakest at station C to M (inner most). The smaller depth of station J is related to its location in a shallower region near a small island. The change of temperature with depth was quite small at all observation stations. Therefore, the density change of the water column was dominated by the salinity which will use as a basic variable in this study. CTD observations were not made during spring tide, the focus of this study, because of the unexpected resignation of the field assistant in charge of CTD profiling and other logistical (poor weather) problems. Stratification during spring tide might have been weaker than the data shown in fig.2.2 due to enhanced mixing. Based on this assumption, the pycnocline depth during the spring tide is

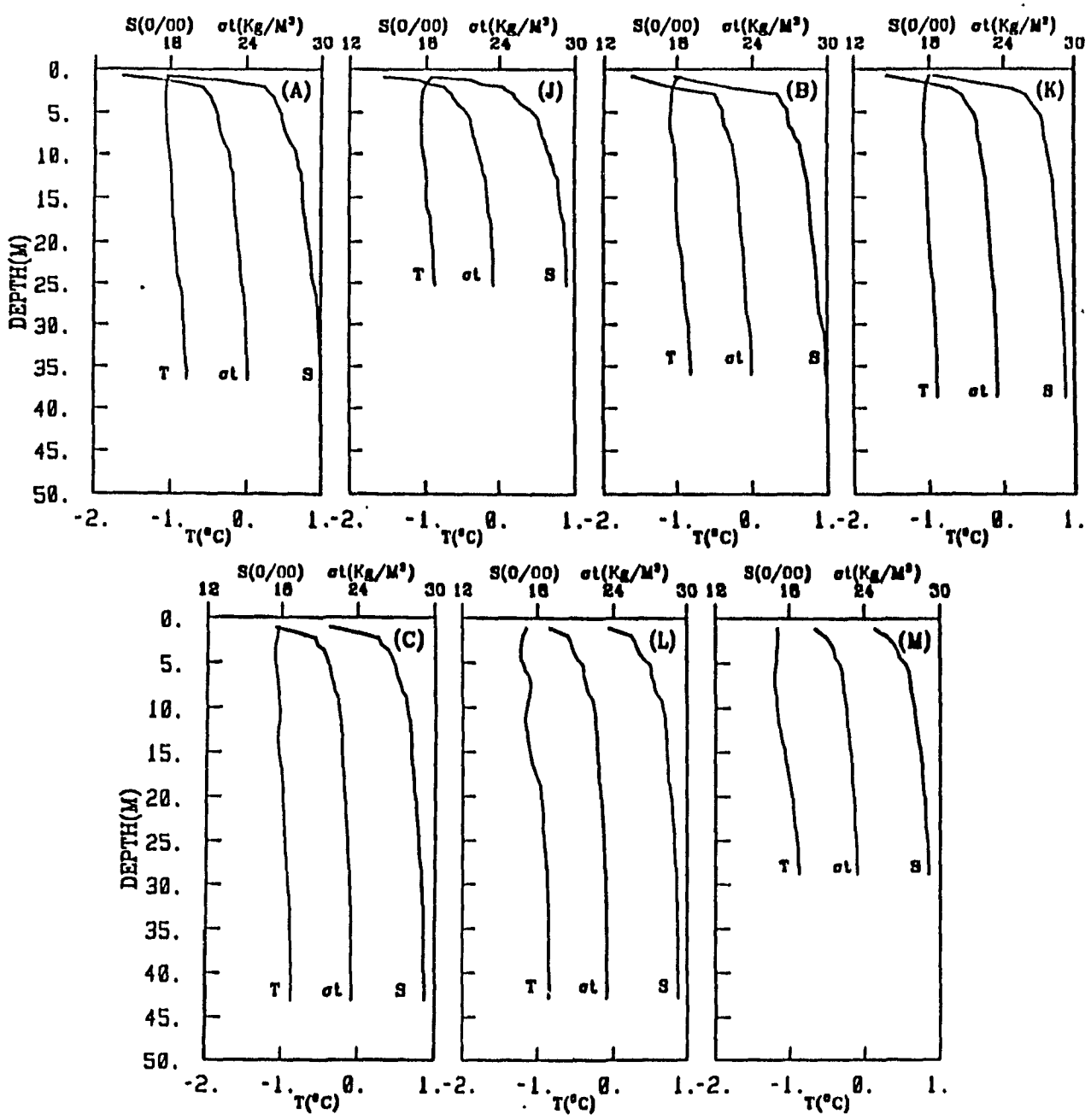

Figure 2.2. Vertical profiles of salinity (S), temperature (T) and density (σ_t) for stations A, J, B, K, C, L, and M on 29 April 1989.

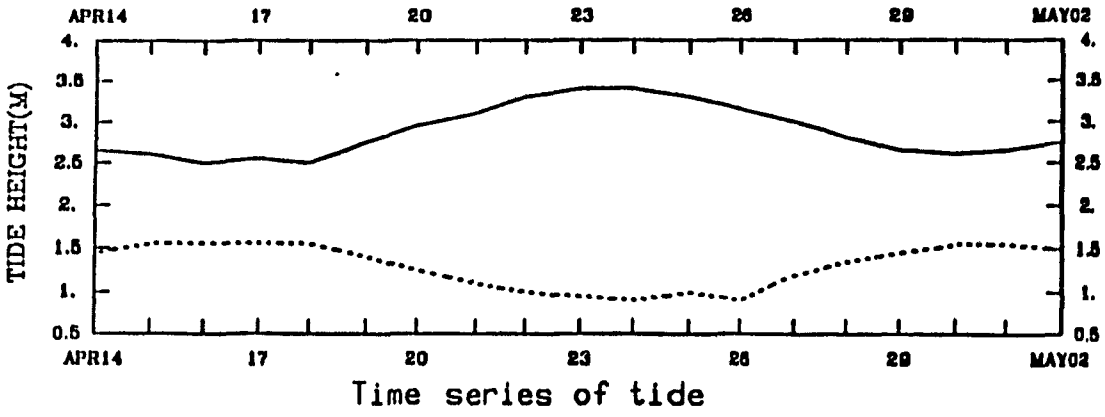

Figure 2.3. Low tide (dashed line) and high tide (solid line) during the observation period based on predictions of the Canada Hydrographic Service.

estimated to be about 3.2, 3.0, and 2.5m under the ice cover for stations A, B, and C respectively, or about 0.5m deeper than at neap tide, similar to the observations of Larouche (1984).

Figs.(2.4-2.6) and (2.7-2.9) present the time series of current, salinity, and temperature for typical neap and spring tides, respectively. Because the cross-sound velocity components were usually much smaller than the along-sound velocity components, and the expected direction of propagation of the internal bores and high frequency waves were also along the channel, the along-channel velocities will be the focus of our study. Here, positive velocities are directed into the sound (NE), corresponding to the flood, and negative velocities are directed out of the sound (SW), corresponding to the ebb. For the cross-channel component, positive velocities refer to NW direction and negative to SE. In figs.2.4 - 2.9, the tidal currents at 2.5m (upper layer) and 7.5 m (lower layer) were generally opposed at station B. However, the whole water column at stations A and C moved in the same direction. The tidal flow was predominantly semi-diurnal in nature. The velocities at station A were much smaller than those at station B (the constriction) or at station C. Maximal velocities reached 60 cm s^{-1} at station B during the spring tide. More variance occurred also in velocity signal at station B than at stations A and C. During neap tide, the velocity was smaller and less variable at the three stations.

Because of a malfunction in the 2.5m deep current meter at station A , no velocity data was recorded. Data at 7.5m for station C were edited to delete a few unrealistic pulses in the velocity signal.

The temperature (T) changes observed at each level and station were small. However, there was a relatively strong rise in temperature (T) at 2.5m for station A, which also accompanied a strong drop in salinity (S) Weaker temperature fluctuations could also be seen at stations B and C. At our observation depths, temperature was in general negatively correlated with salinity. Although the temperature gradually decreased with depth, surface values were at or near the freezing point due to the lower salinity values of

the water. The average temperature and σ_t are listed in Table 1.

Examining the along-channel salinity field, we found that there was a rapid salinity increase in the upper layer as the spring tide began, and reached a maximal value on 26 April. The lowest salinity was at station A, with the highest at station C, as shown in figs.2.10 and 2.11. Most of the salinity difference between downstream and upstream stations (ΔS) in fig.2.11 was positive; however, a slight decrease occurred at 2.5m for stations A to B during spring tide period.

At the time scale of the semidiurnal tide, fluctuations in salinity were prominent at the upper two observation depths during both neap and spring tides (fig.2.4-2.9,(e)). At station A, there were large drops in S at 2.5m through the neap and spring tide, when the tide changed from flood to ebb. In comparison, salinity at 1.5m and 7.5m was nearly constant.

For station B, during the spring tide, salinity at 2.5m increased gradually, from the beginning of ebb and reached its maximal value at the following flood peak. During the interval from peak flood to the beginning of ebb, salinity dropped steadily in the initial stages, then increased sharply, gaining about 6 o/oo in a few minutes. Strong salinity bores were superimposed on the tide signal. High frequency variation of salinity was generated during spring tides from some of these strong salinity bores, as the tide shifted from flood to ebb. Similar but weaker signals were also observed at 1.5m. Thus, the salinity variations at the upper layer of station B can be characterized by a bore/drop and high frequency waves. In contrast, the salinity at 7.5m was quite stable.

During spring tides at station C, a strong bore of salinity at 1.5m, followed by a drop at 2.5m, occurred during the flood (fig.2.9). A very weak fluctuation also appeared in the temperature field but not in velocity at 1.5 and 2.5m. The large fluctuations at 7.5m are thought to result from uncertainties in the data caused by a current meter malfunction. The temperature difference between observed depth was smaller than that at the

TABLE 1

		Neap Tide			Spring Tide		
Instrument depth		1.5	2 5	7.5	1 5	2.5	7 5
T (^{0}C)	A	-0.7	-1.0	-1 1	-0.8	-1.0	-1.0
	B	0.1	-0.9	-1.1	-0.1	-0.9	-1.1
	C	-0.8	-0.9	-1.1	-0.9	-1.0	-1.0
σ_t (kg/m^3)	A	9.3	15.8	21 7	12.0	17.0	22.1
	B	10.9	16.0	21.9	12.6	17.1	22.1
	C	13.1	17.6	21.8	14.5	19.1	22.9

Table 1. The average temperature and σ_t for three stations at current meter depths.

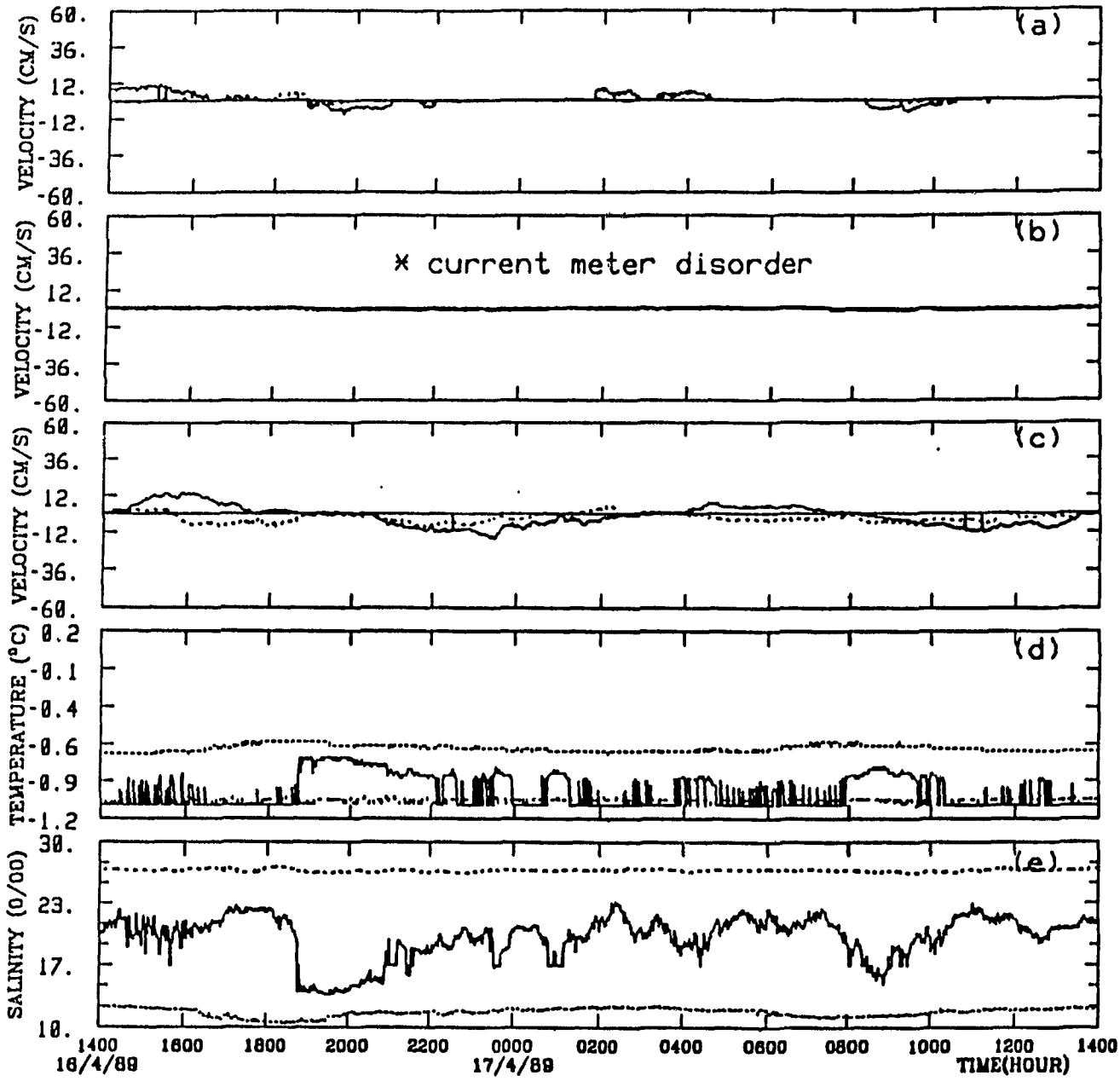

Figure 2.4. Time series of current, temperature and salinity at station A during neap tide. (a),(b) and (c) are the velocity at 1.5, 2.5 and 7.5m respectively, in which solid and dashed lines represent along- and cross-sound component, respectively. (d) and (e) are the temperature and salinity, in which dashed, solid and dotted lines represent the value at 1.5, 2.5 and 7.5m respectively.

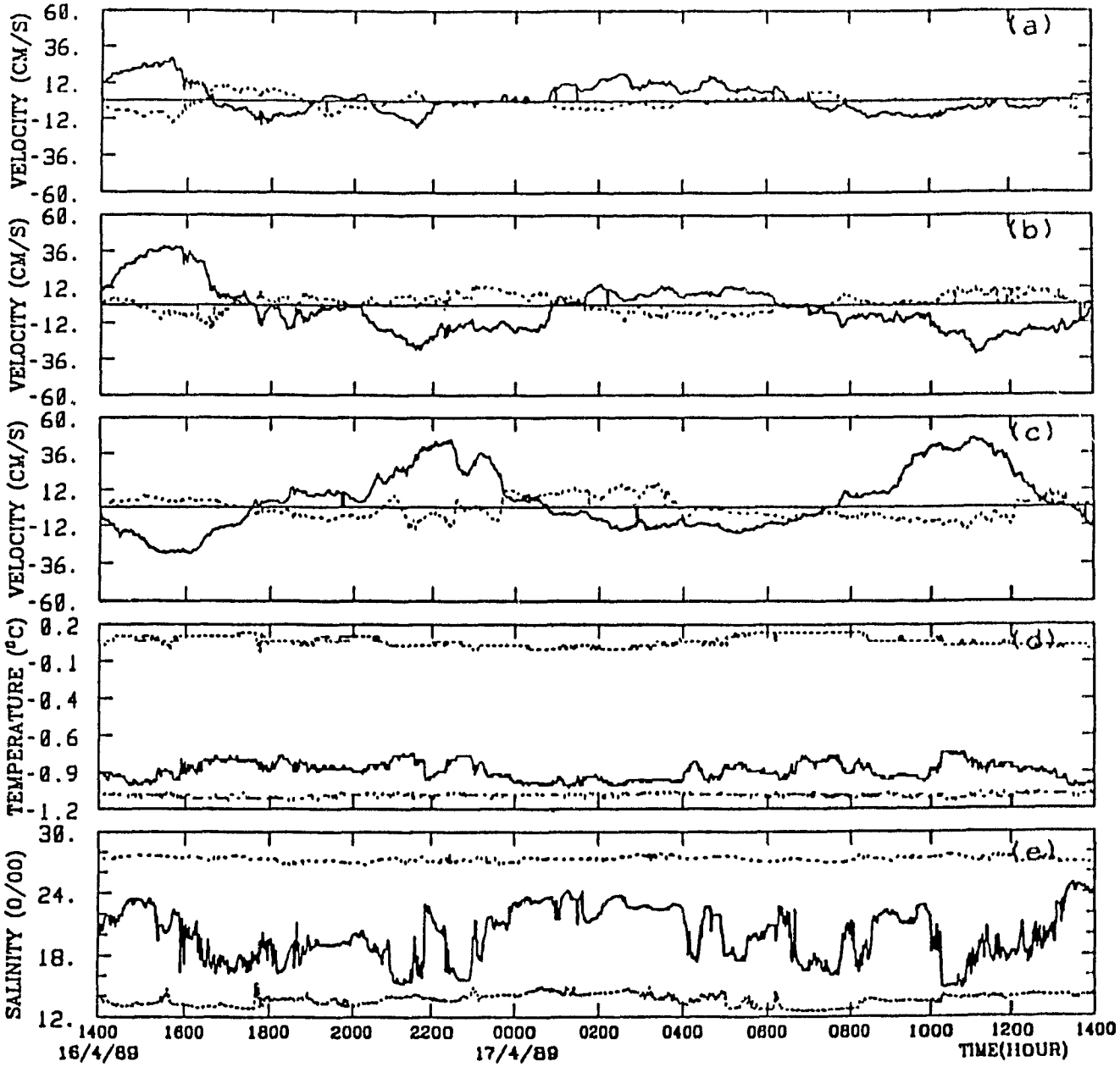

Figure 2.5. Time series of current, temperature and salinity at station B during neap tide. (a),(b) and (c) are the velocity at 1.5, 2.5 and 7.5m respectively, in which solid and dashed lines represent along- and cross-sound component, respectively. (d) and (e) are the temperature and salinity, in which dashed, solid and dotted lines represent the value at 1.5, 2.5 and 7.5m respectively.

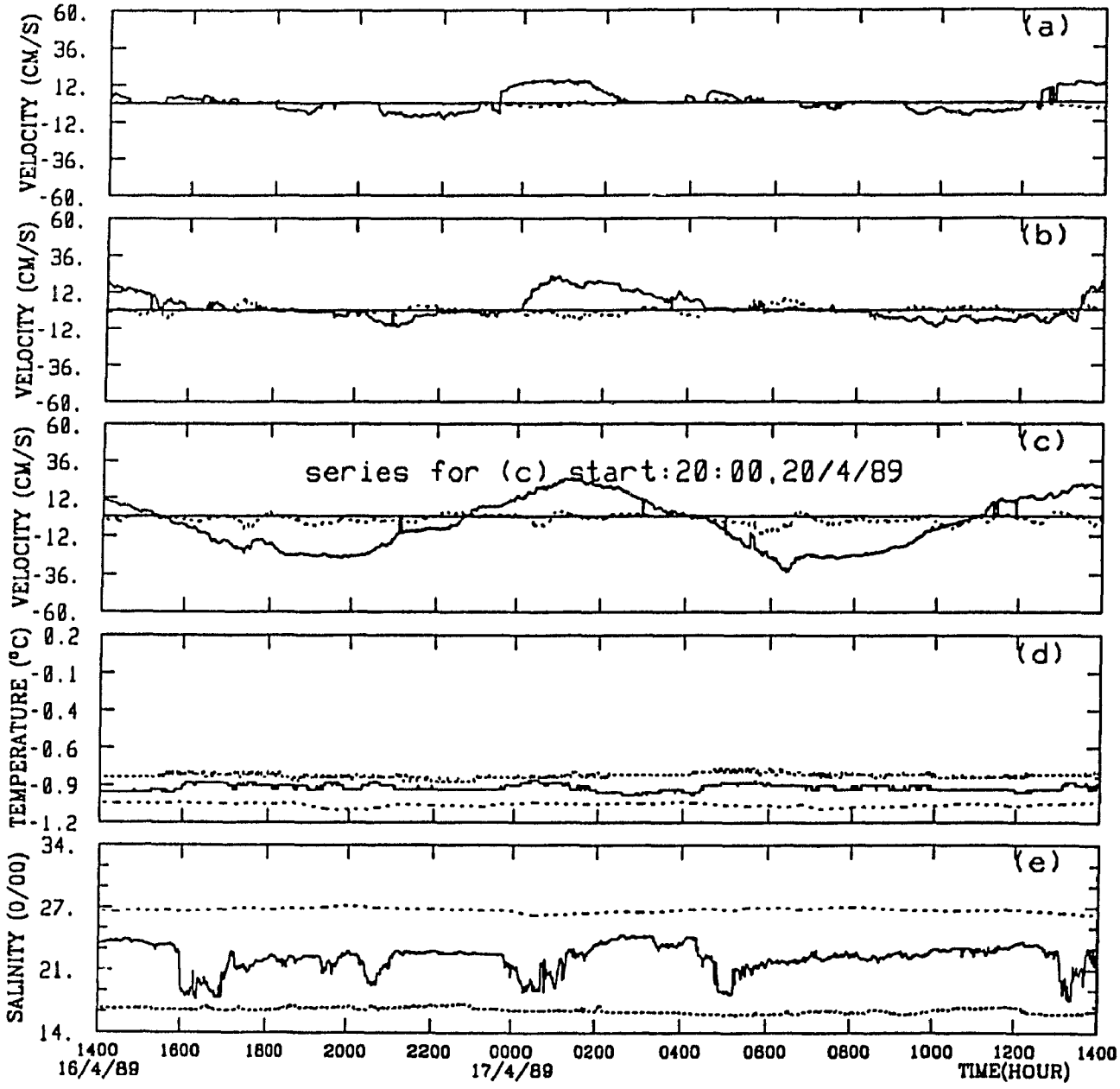

Figure 2.6. Time series of current, temperature and salinity at station C during neap tide. (a),(b) and (c) are the velocity at 1.5, 2.5 and 7.5m respectively, in which solid and dashed lines represent along- and cross-sound component, respectively. (d) and (e) are the temperature and salinity, in which dashed, solid and dotted lines represent the value at 1.5, 2.5 and 7.5m respectively.

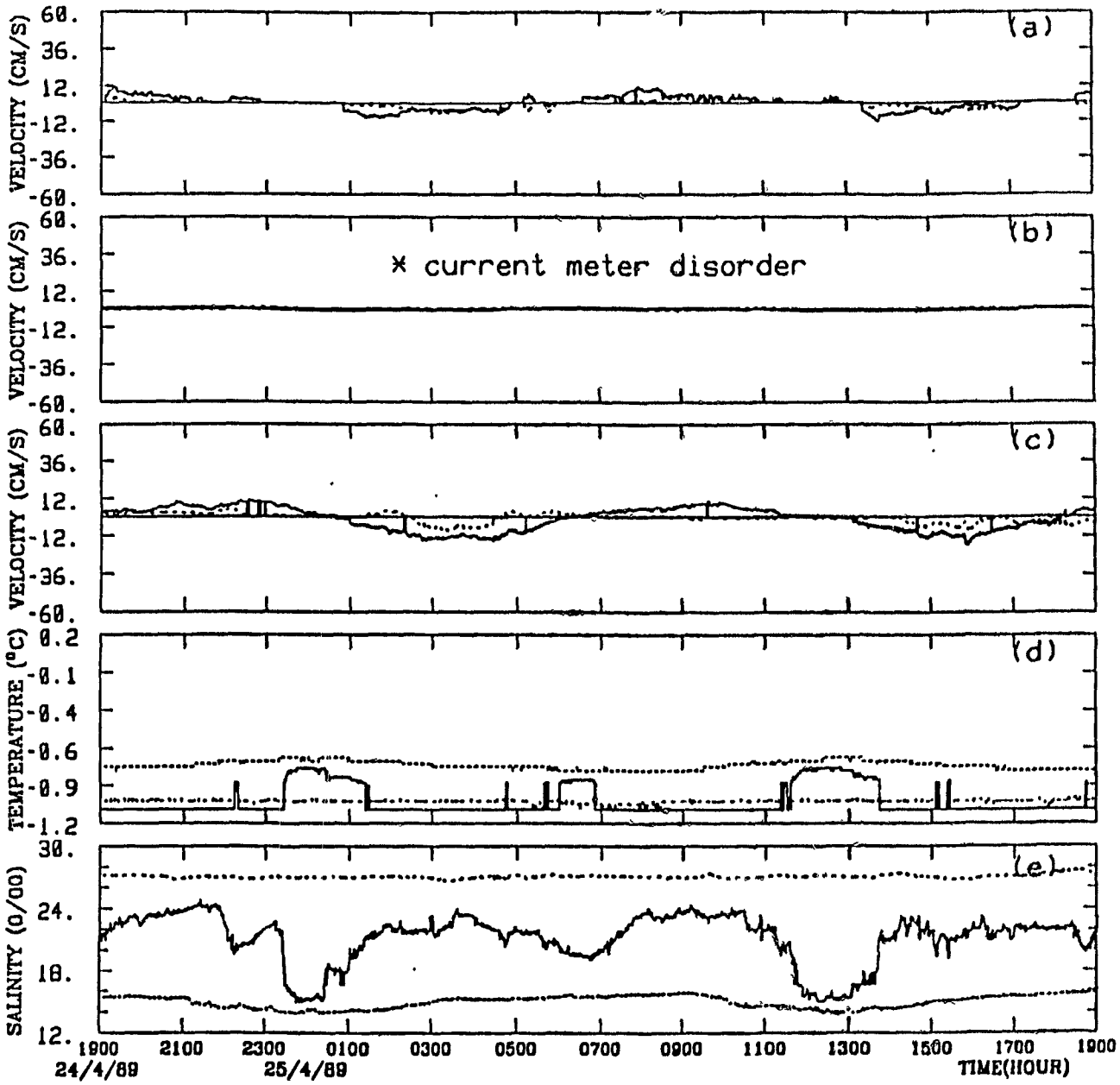

Figure 2.7. Time series of current, temperature and salinity at station A during spring tide. (a),(b) and (c) are the velocity at 1.5, 2.5 and 7.5m respectively, in which solid and dashe lines represent along- and cross-sound component respectively. (d) and (e) are the temperature and salinity, in which dashed, solid and dotted lines represent the value at 1.5, 2.5 and 7.5m respecttively.

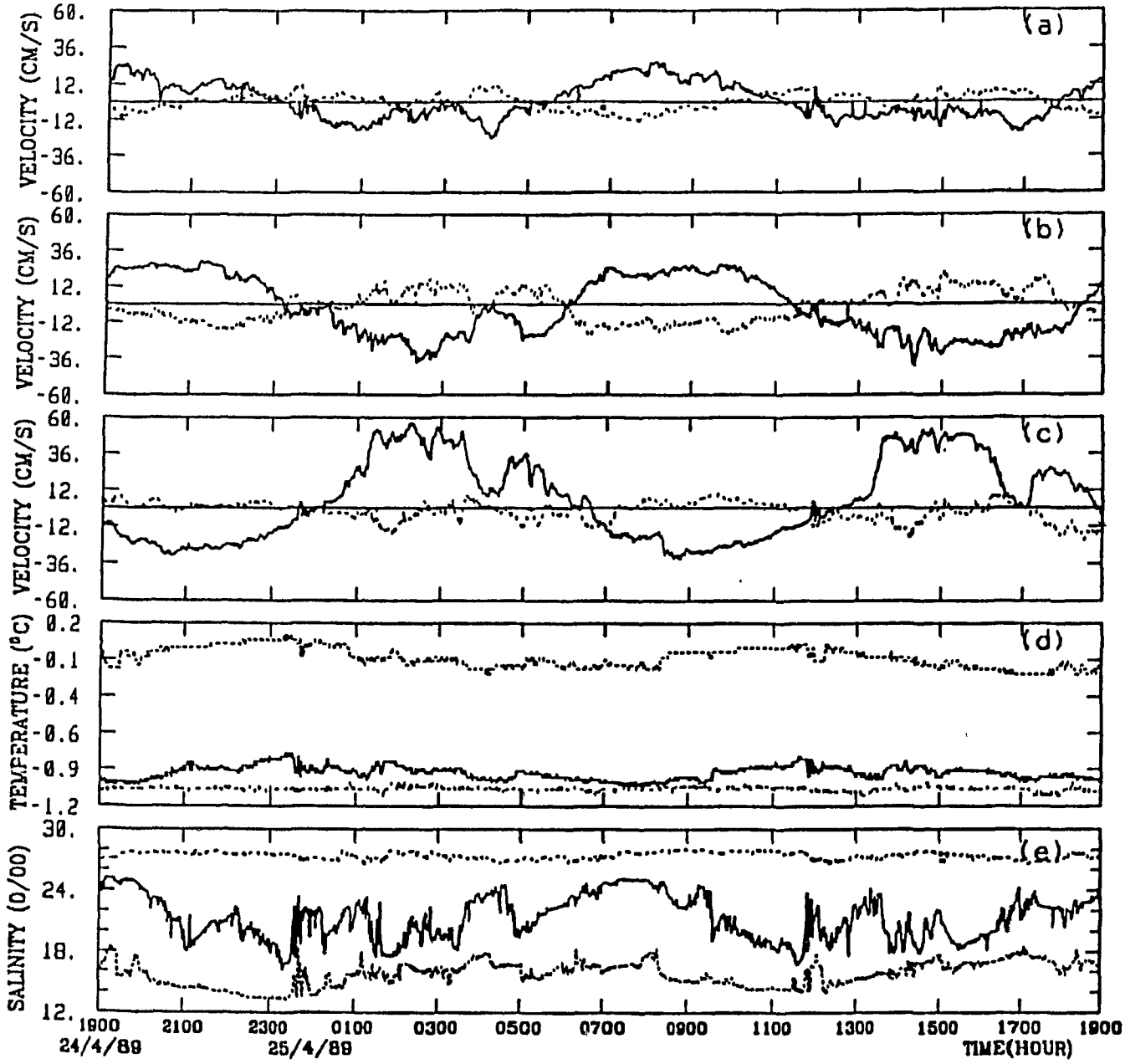

Figure 2.8. Time series of current, temperature and salinity at station B during spring tide. (a),(b) and (c) are the velocity at 1.5, 2.5 and 7.5m respectively, in which solid and dashed lines represent along- and cross-sound component, respectively. (d) and (e) are the temperature and salinity, in which dashed, solid and dotted lines represent the value at 1.5, 2.5 and 7.5m respectively.

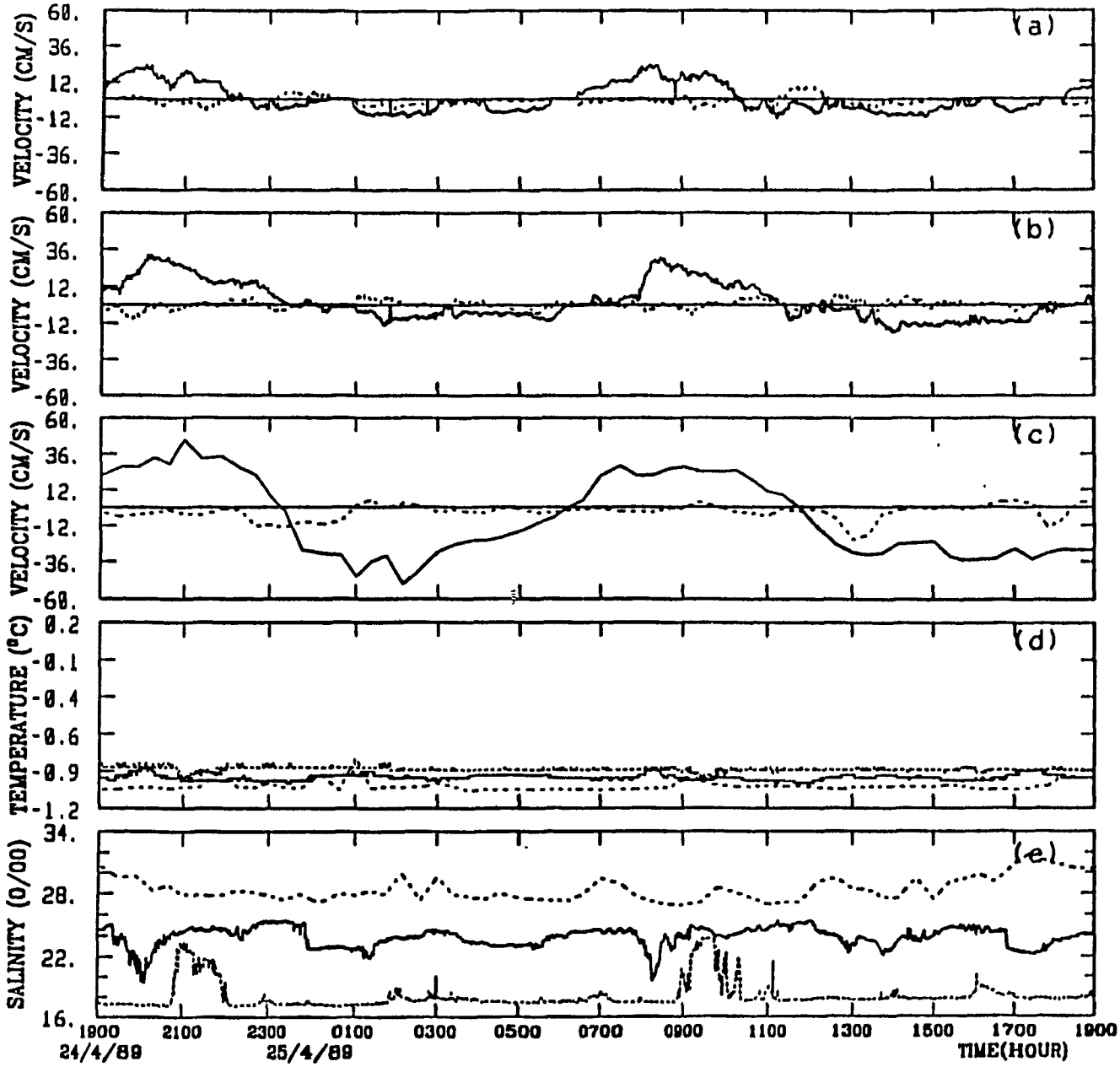

Figure 2.9. Time series of current, temperature and salinity at station C during spring tide. (a),(b) and (c) are the velocity at 1.5, 2.5 and 7.5m respectively, in which solid and dashed lines represent along- and cross-sound component, respectively. (d) and (e) are the temperature and salinity, in which dashed, solid and dotted lines represent the value at 1.5, 2.5 and 7.5m respectively.

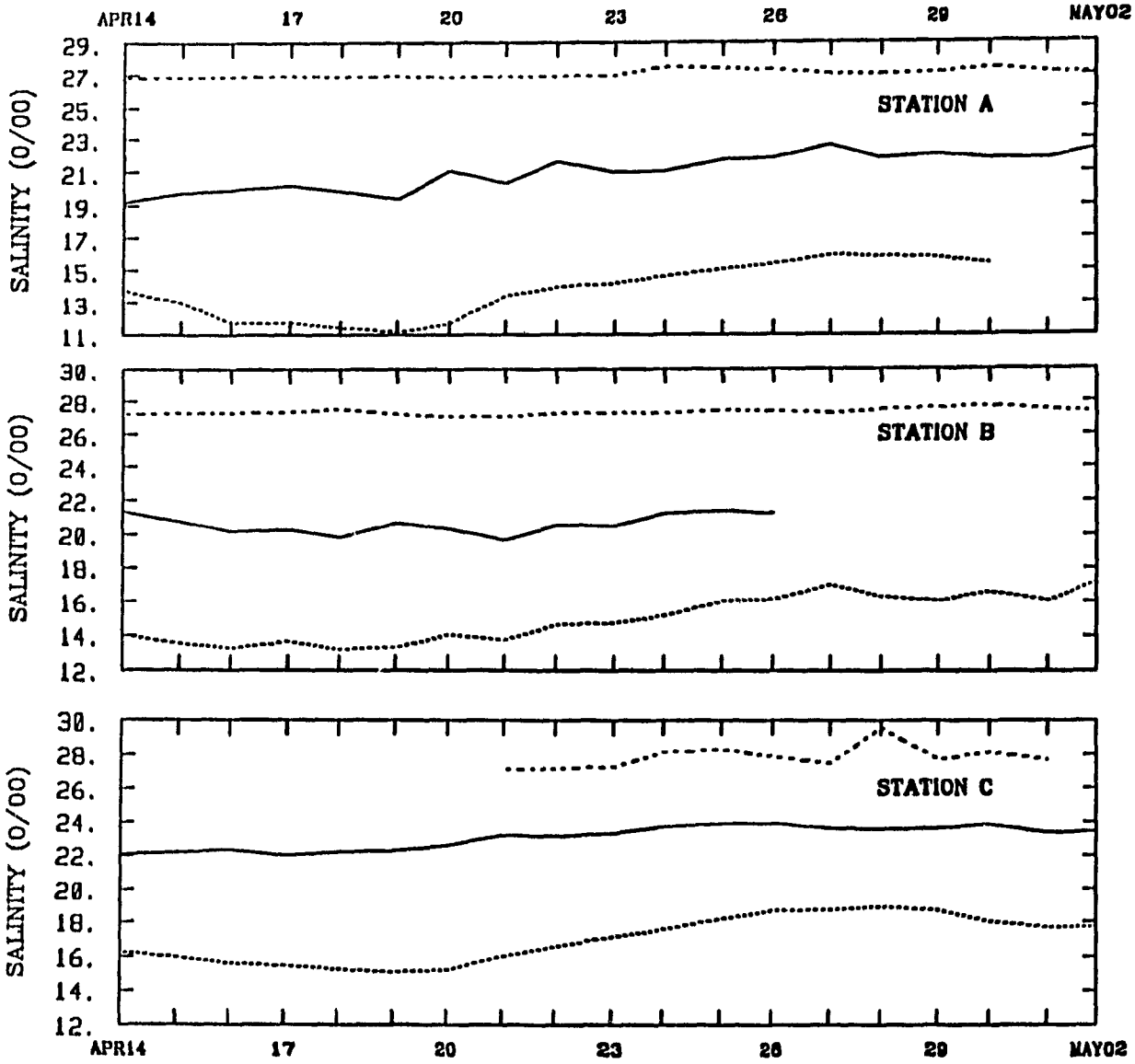

Figure 2.10. The time series of salinity at station A ,B and C after averaging to remove semi-diurnal and diurnal variability. Dashed, solid and dotted lines refer to 1.5, 2.5 and 7.5m respectively.

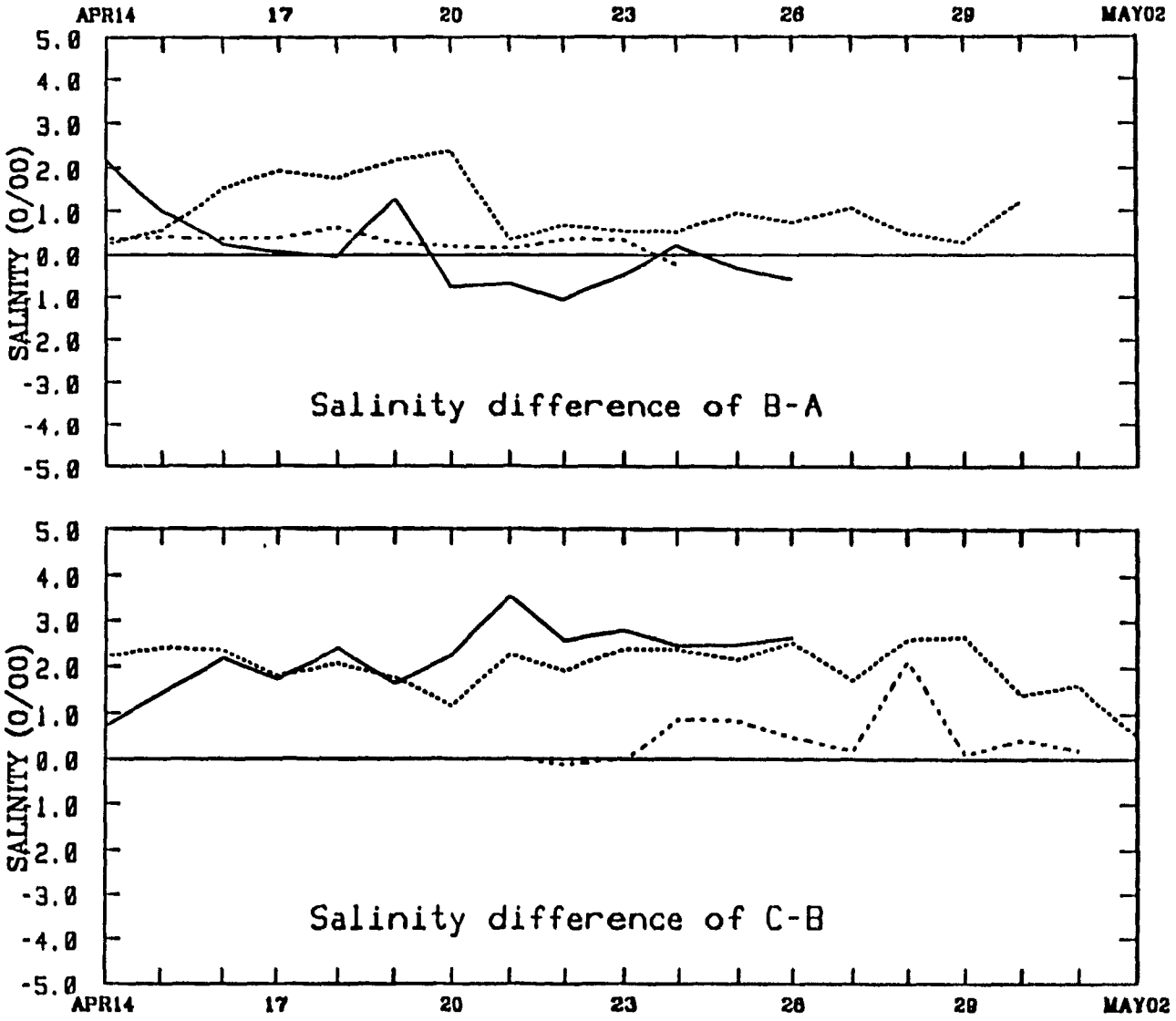

Figure 2.11. Time series of salinity difference between station B and A(a), and station C and B (b). Dashed, solid and dotted lines refer to 1.5, 2.5 and 7.5m respectively.

other two stations. During the neap tide, the strong bore at 1.5m disappeared and the drop at 2.5m was much weaker than that during the spring tide.

Assuming linear salinity gradients between measured points and conservation of salinity, the computed isohaline contours from 1.5-7.5m are shown in figs.2.12 and 2.13. The effect of the internal drop at station A extended from the surface to about 6.5m during both spring and neap tide. The maximal drop of 3-3.5m amplitude occurred at a depth of about 3m during the spring tide and a depth of 2.5m during the neap tide (estimated from 22 o/oo contour). At station B, the high frequency wave signals extended from the surface to a depth of 5.5m during the spring tide. The maximum high frequency wave depression dropped from a depth of 2.5m to 4.5m (contour 21.6 o/oo contour). The drop at station C, shown in (c) of both figs.2.12 and 2.13, occurred over a depth range of 2.0 - 6.5m depth. The drop during neap tide was smaller than during spring tide.

We can also see from figs.2.12 and 2.13 that the strongest vertical salinity gradient is located between 1.5 and 2.5m. This strong gradient was sharper during neap tides, and weakened during the spring when hydraulic drops or bores occurred. Similar to the result from the CTD profiles, the pycnocline depth was deeper during the spring tide. Note, the pycnocline was also deeper during the presence of internal bore, drop and solitary waves.

Similar to the high-frequency internal oscillations in salinity at station B, fluctuations in temperature and velocity were also observed when the upper layer tide changed from flood to ebb. The presence of very small vertical gradient of temperature and velocities between 2.5 and 7.5m during the period of high frequency fluctuations does not allow easy identification of the high-frequency signal in both temperature and velocity records. The high frequency fluctuations appeared very much like the decomposition of a bore perturbation into a sequence of high frequency waves. For the stratification in the sound, the waves must have been of the depression type. The periods of the waves were estimated at about 2-6 min., which was slightly longer than the suggested values of 2-3 min. by Ingram et al (1989). The

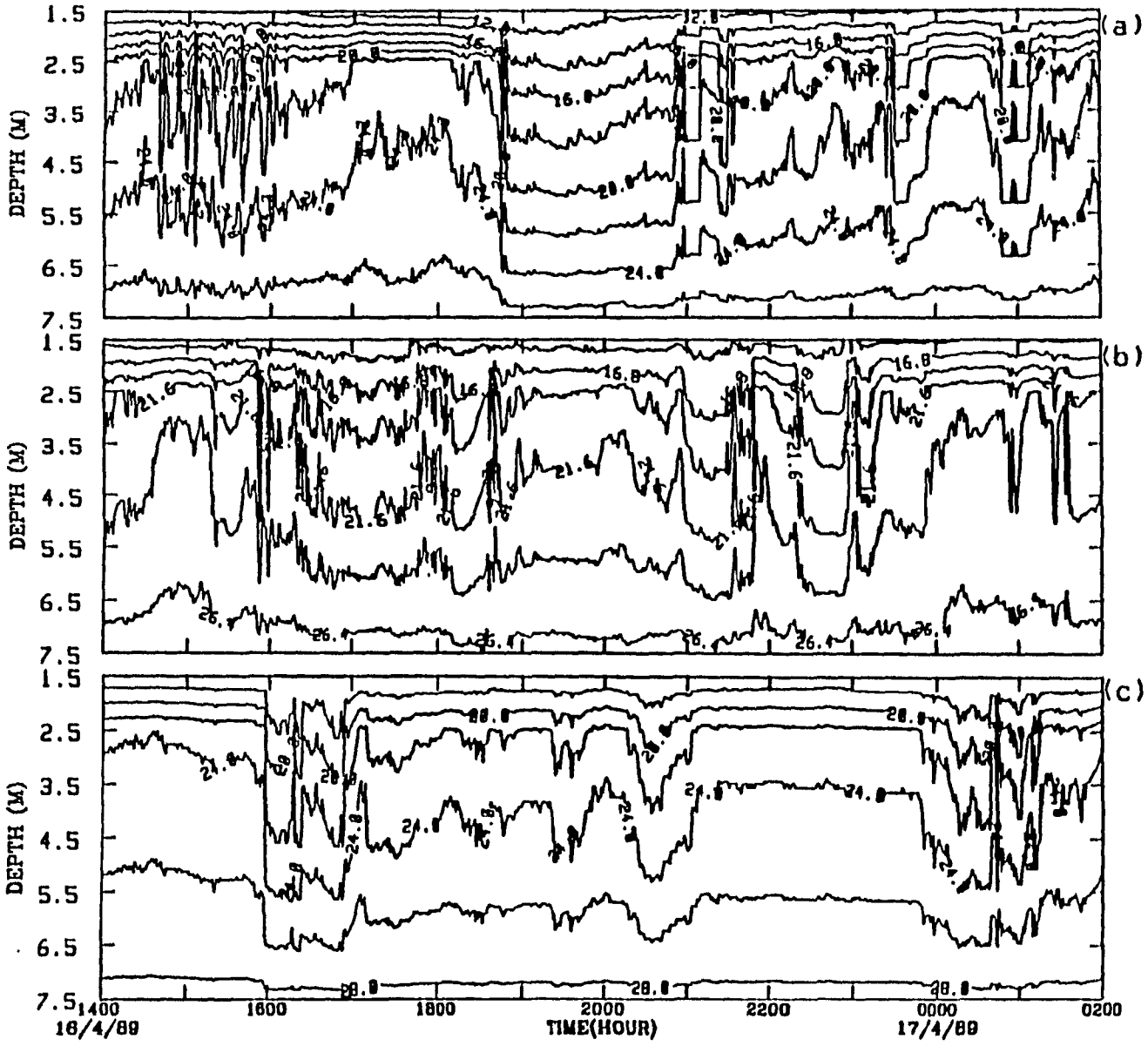

Figure 2.12. The computed contours of constant salinity based on an interpolation of observations at discrete depths at stations A(a), B(b) and C(c) during the neap tide.

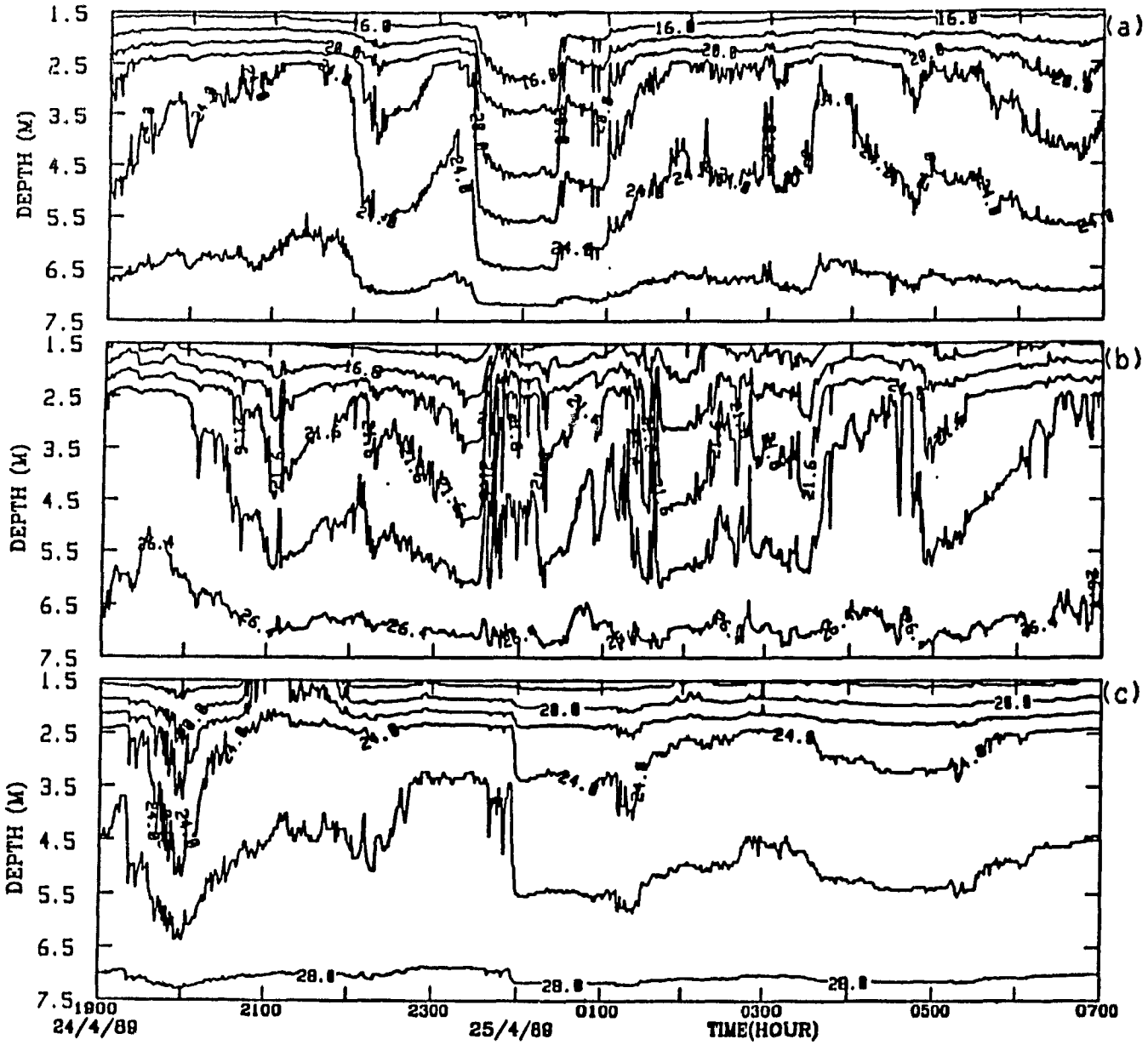

Figure 2.13. The computed contours of constant salinity based on an interpolation of observations at discrete depths at stations A(a), B(b) and C(c) during the spring tide.

oscillations were in a packet of approximately six in number with the largest arriving first. The oscillations are thought to be solitary waves. Their amplitude, based on the salinity gradient was approximately estimated from the equation:

$$AMPLITUDE_{soliton} = \frac{\Delta S}{(\frac{\partial S}{\partial Z})} \qquad (1.1)$$

under the assumption that the horizontal salinity advection is small. In (1.1), ΔS is the salinity increase due to crest steepening of the wave and $\partial S/\partial Z$ is the salinity gradient. The amplitude (peak-trough) in our case was estimated as about 2-3m. This method seemed to be a more satisfactory procedure to estimate wave amplitude than computing contours of constant salinity based on an interpolation of observations at discrete depths, particularly since the time series measurements only covered the depth range 1.5-7.5m, and individual water masses could not be traced to obtain the wave amplitude. On the other hand, because of abnormally lower winter run-off of the Great Whale River during the observation period($\approx$100 m^3/s) in 1989 compared to other years, the stratification was weaker than normal. Hence, both hydraulic bore/drop and solitary waves may have differed during years of stronger river discharge .

Individual bores and solitary wave events were not followed between mooring stations. Station spacing was too great to observe the solitary wave signal before it dissipated. Thus the data could not provide a measure of the phase speed nor the direction in which the wave propagated. In fact, it could only be deduced from the data at station B that the propagation was mainly in the upstream direction, i.e. towards to the entrance of the sound.

Chapter 3. Internal Hydraulic Jumps

3.1 Introduction

A two-layer hydraulic theory is used to characterize the flow through the constriction. First, theory and some of the relevant properties of internal hydraulics are introduced. Then, the possible internal hydraulic configurations in the sound are discussed based on hydraulic theory. Discussions in this section will use the two-layer model as the best approximation and focus on the spring tide period.

3.2 Internal Hydraulics

The fluid in a channel can be described by the momentum or Bernoulli's equation as it moves through the narrowest section or over a sill (Long,1955). By combining Bernoulli's equation with the continuity equation, it can be shown that changes in fluid depend on the internal Froude number, defined by

$$F^2=U^2/(g'h) \qquad (3.1)$$

where h(x) and U are the depth and velocity of fluid along the channel, respectively and g' is reduced gravity. The internal Froude number, F, as defined by equation (3.1), is the ratio of kinetic (KE) to potential energy (PE) of the fluid. When $F^2=1$, the flow is called critical and corresponds to the state in which the velocity of the fluid equals the velocity of an infinitesimally small amplitude long wave on the layer. Similarly, for $F^2>1$ or $F^2<1$, the flow is called internally supercritical or subcritical, respectively. Based on the concepts of energy from Bernoulli's equation and of mass conservation from the continuity equation, if the flow is subcritical upstream and critical at the sill or narrowest section, it will be supercritical downstream of the sill or narrowest section. Supercritical flow downstream can match to the subsequent subcritical flow by the presence of an internal hydraulic bore or jump. The physics involved in these processes

can be described as follows: for the flow over a sill, the fluid elements obtain PE at the crest and transfer PE to KE when they are driven by the downward buoyancy force. This KE can, in turn, cause each element to overshoot its equilibrium level (jump) and may also have a series of oscillations. Similarly, when fluid particles approach the narrowest section, they are accelerated, thereby increasing the KE. If the flow moves from the subcritical region, this may result in critical flow (i.e.$F^2=1$) at the narrowest section, and supercritical downstream. To further understand this process, the Bernoulli equation (for single layer):

$$\frac{U^2}{2g}+h=constant \tag{3.2}$$

and continuity equation

$$Q=Uhb=constant \tag{3.3}$$

is combined to

$$\frac{Q^2}{2h^2b^2g}+h=constant \tag{3.4}$$

here b and Q is the width and discharge in the sound. Thus, differentiating equation (3.4) with respect to x,

$$(1-\frac{Q^2}{gh^3b^2})\frac{dh}{dx}-\frac{Q^2}{gh^2b^3}\frac{db}{dx}=0 \tag{3.5}$$

or

$$(1-\frac{U^2}{gh})\frac{dh}{dx}=\frac{U^2}{gb}\frac{db}{dx} \tag{3.6}$$

It is apparent that the flow can be critical ($F^2=1$) only where $db/dx=0$. If we differentiate equation (3.6) with respect to x, we get

$$(1-\frac{U^2}{gh})\frac{d^2h}{dx^2}+\frac{U^2}{gh^2}(\frac{dh}{dx})^2=\frac{U^2}{gb}\frac{d^2b}{dx^2}-\frac{U^2}{gb^2}(\frac{db}{dx})^2 \qquad (3.7)$$

When it is critical at the narrowest section, the first term on the left and the second on the right vanish. Since d^2b/dx^2 is not equal to zero at the narrowest section, dh/dx does not vanish at the narrowest section. Hence, if it is subcritical upstream and critical at the crest, it will be supercritical just out of the narrowest section due to the negative dh/dx (i.e. decreasing water depth h(x)). The same method can also apply to flow having supercritical upstream and to internal flow.

Earlier studies on internal hydraulic jumps downstream of the control include that by Benton (1954) based on the principles of momentum conservation and later revised by both Yih and Guha (1955) and Mehrotra (1973). In his studies, Long (1954) showed results of various possible fluid configurations over an obstacle from initially uniform flow upstream and downstream. However, the first study of the two-layer flow, in which both layers interact and play a significant role in the establishment of control of the flow, was by Stommel and Farmer (1953). Some of their results were later verified by Armi and Farmer (1985), who used the simpler conservation-energy equations and treated the flow by parameterizing in terms of the internal Froude number for each layer to predict the conjugate state for an internal hydraulic jump under the influence of two-way hydraulic control. Specifically, Armi and Farmer (1985) described how a sill or constriction affected the exchange of flow in a channel. They emphasized the importance of the net barotropic flow in the two-way exchange and elucidated the basic difference between maximal and submaximal two-layer exchange flows. Their findings showed that the flow was internally critical not only at the control section of the sill or narrowest section, but also at a location called the virtual control section (when flow

is at maximal exchange and a net barotropic forcing exists). The barotropic forcing exists if

$$q_r=Q_1/-Q_2\neq 1 \qquad (3.8)$$

according to Armi and Farmer(1985). The Q_i (i=1,2) are the discharge in each layer as defined in equation (3.3). The requirement for maximal exchange is that supercritical flows occur on both sides of an exchange control. If only one supercritical flow exists, the control would be submaximal. According to Armi and Farmer (1985), the necessary condition for an asymmetrical interface under steady conditions is that the flow undergo the critical condition ($G^2=1$) for two-layer flow. Where the G^2 is defined by a composite Froude number:

$$G^2 = F_1^2+F_2^2 \qquad (3.9)$$

Using a similar method for a three-layer model, Farmer and Denton (1985) showed the existence of the "approach control". It was located downstream of the sill crest unlike "normal control" which occurred at the sill. The combined effect of a sill and a constriction was also discussed by Farmer and Armi (1985). A similar problem was discussed by Hogg (1985) who found that the width constriction was subject to the slowest, second internal mode control while the combination of sill and constriction is subject to the first mode control. Baines (1984) has combined hydraulics with nonlinear wave theory to a study of the upstream bore and found that bores are governed by nonlinear effects and their character was determined by a balance between nonlinear steepening and dispersion of the wave.

Although the basic method used for studying single-layer and two-layer flow is quite similar, two-layer flows have a quite different response over a sill and in narrow sections. Farmer and Armi (1985) also showed the control at the sill crest acts primarily through the deeper layer into which it protrudes, and only indirectly controls the surface layer.

3.3 Discussion

Fig.3.1 (a and b) shows the internal Froude number at stations B and C throughout the tidal cycle, corresponding to the time series in figs.2 7-2 9.

The Froude number was calculated by using the current meter data at depths of 2.5m and 7.5m. The G^2 values in fig.3.1 were averaged over 12 min. intervals to delete high frequency fluctuations. For the three stations, F_2^2 was approximately equal to zero due to the deep lower layer. Consequently, composite Froude numbers G^2 were dominated by the upper layer Froude number (i.e. $G^2 \approx F_1^2$). Therefore, the lower layer was essentially passive at all three stations. Froude numbers at station A were close to zero. The time-dependence of G^2 implies that the hydraulic control along the sound varied during the tidal cycle. Two conditions approaching critical ($G^2=1$) or even supercritical flows happened at station B at the time of maximum flood (inflow of upper layer). Supercritical flow occurred at station C, just after maximum flood, and may indicate a control downstream of the narrowest section as will be discussed subsequently. The corresponding side and plan view of the two-layer hydraulic control flow through the constriction and small island are shown in fig.3.2 for spring tide. The figure shows three possible interface configurations from our data set at different stages of the tide. These are based on the time series of Froude number along the sound in fig.3.1 and two-layer hydraulic theory. Our aim is to explain the periodic bores (or drops) and interface tilt along the sound (figs. 2.7-2.9).

Case 1, shows conditions two hours before maximal flood. The critical condition occurred at the narrowest region with subcritical conditions at both stations A and C. Just downstream of station B, supercritical conditions were highly likely because of the effects of constriction control (see the discussion of equation 3.7). As the flow moved to $F_1^2>1$, the interface rose (i.e. h_1 decreased). After the flow passed the region of $F_1^2<1$, the bore was generated. This can be proved for the corresponding bore shown at station B (fig.2.8). The bore at station B can be thought of as resulting from upstream propagation as the flood tide weakened and turned to ebb. The bore could also occur during the ebb, if critical at the narrowest section and supercritical conditions at upstream of the narrowest region were reached. However, this condition might not happen because bores were observed at station B only

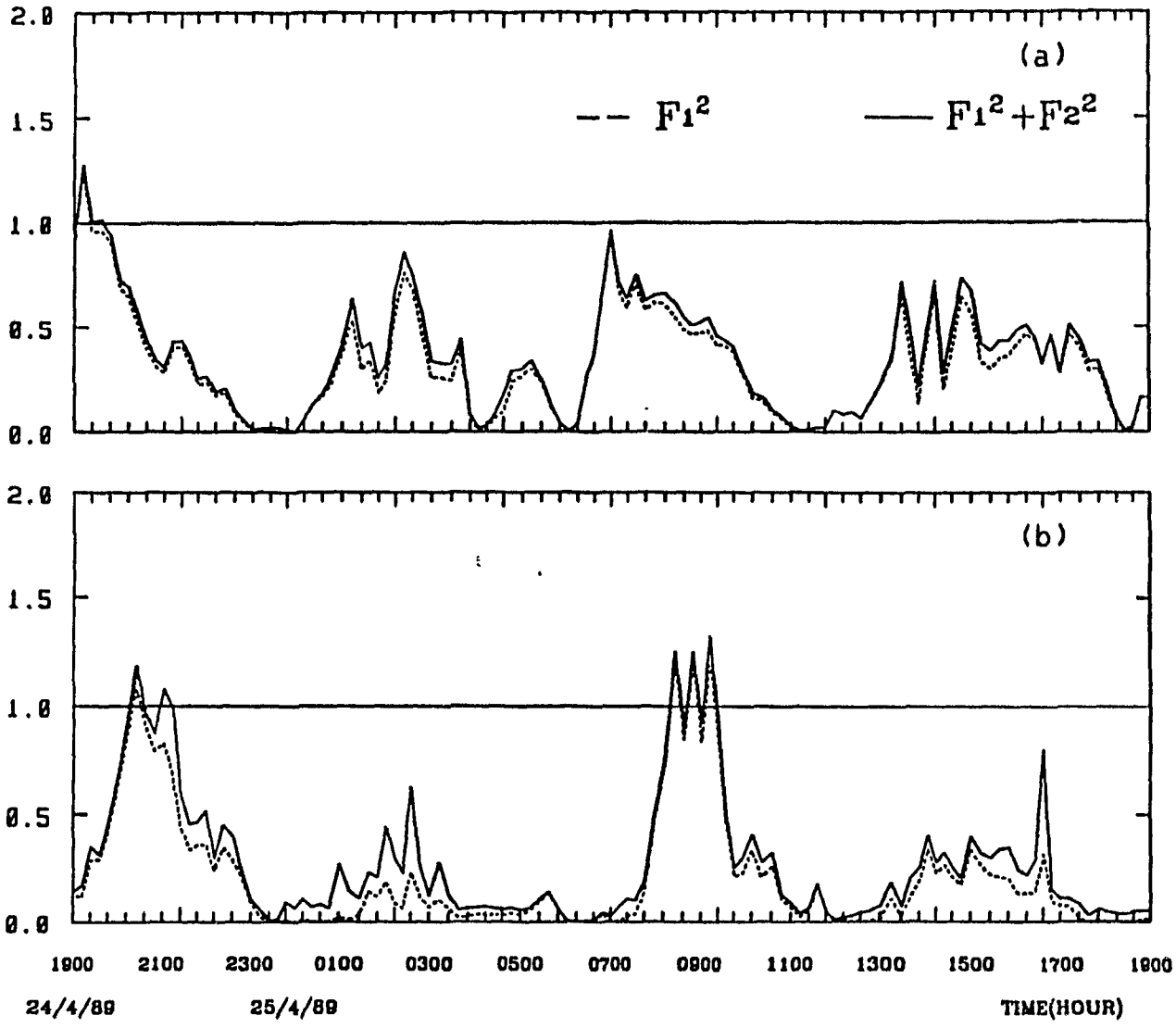

Figure 3.1.Time series of composite Froude number at station B(a) and station C (b) on 24 and 25 April 1989. The Froude number in station A was close to zero.

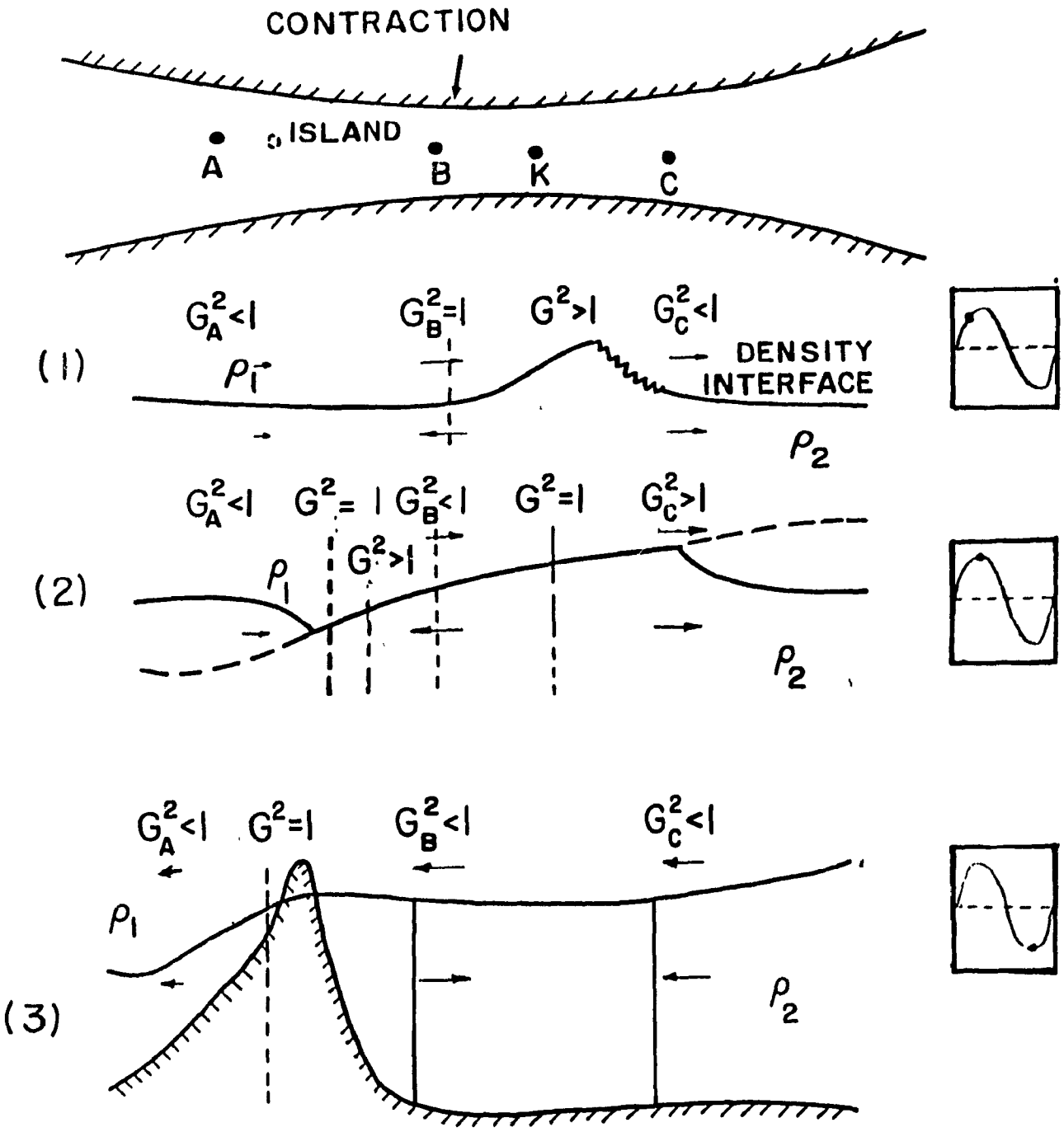

Figure 3.2. Plane and side view of four possible interface configurations in the Manitounuk Sound during spring tide, at different tide stages. The sill in (1) and (2) is neglected in figure.

during ebb, i.e. only from downstream of station B.

Case 2 corresponds to the condition at maximal flood. Supercritical conditions occurred at station C. Since the flow upstream was subcritical, there must be a continuous transition from subcritical to supercritical flow downstream. The one hour lag between the time of critical flow at station B and supercritical conditions at C signified that the critical condition matching to supercritical condition at station C might occur between stations B and C instead of at B. This critical condition resulted from the control at narrowest section which could have caused the upper layer downstream to approach critical conditions by shallowing the upper layer asymptotically. A bore was generated and can be seen from the salinity time series at station C (fig.2.9). The shallower interface near station C resulted in the bore being found at the 1.5m level instead of at the lower level. At the downstream side of the small island near station A, the slope of the sill-like feature may greatly reduce the total water depth (the total depth near the island was less than 10m). During the flood, the shallower area near island may have increased F_2^2 dramatically, and hence resulted in critical and supercritical flow. When the flow matched subcritical flow downstream, the drop was generated. It is the relaxation of flood that allows the drop to move back upstream. The flattening of drop trough recorded in station A (figs.2.4 and 2.7) also implied the pycnocline was close to the bottom. Similarly, a drop was generated at opposite tidal phase, westward of the small island (case 3). The drop travelled eastward when the flood started. Since the drop westward of small island during ebb didn't pass but was only close to station A, a much weaker drop signal was recorded at station A. The drops shown at 2.5m depth at both station B and C (figs. 2.8 and 2.9) can be thought to be the result of downstream propagation of a drop from station A when the tide slackened and turned to flood. Time series observations of the internal drop as it travelled downstream, showed that it always arrived at about the same tidal phase for both station B and C. If we approximate the bore propagation speed by the phase speed of a nonlinear wave (see next chapter), the time when the

drop appeared at station B was equal to the arrival time of the drop propagating from station A. However, the propagation towards station C from B might take longer time since the subsequent ebb will reduce the travel speed of drop. During the neap tide, the smaller tidal currents might result in a correspondingly different arrival time, as shown in figs.2.5 and 2.6. Since the drops were generated upstream, they were more apparent at the 2.5m level, closer to the interface height in those areas. Thus, the drop shown at station C would have appeared closer to the 2.5m instead of the 1.5m layer.

At the beginning of the ebb (between case 2 and 3), there were no controls along the sound. The bores generated downstream during case 1 and 2 were passing through station B by this time. Some of the arrival bores were released to form a high frequency internal wave train propagating continuously upstream, as will be discussed in next chapter.

It should be noted that the bore was generated when the upper layer flow moved towards supercritical region (i.e. decrease h_1), and the drop occurred when the lower layer moved towards the supercritical region (i.e. decrease h_2).

The conditions of two supercritical flows, with a subcritical flow between these two regions within the sound (case 2), demonstrated that the exchange was maximal. The hydraulic processes depended only on the conditions between these two bounding supercritical areas. However, both cases (1) and (3) are characterized as submaximal exchange, and will always be influenced by one of the reservoir conditions (Armi and Farmer, 1985). This reservoir interface height must allow a bore to exist, move back into, and flood the control (Armi and Farmer, 1985).

The theoretical results, both for bore generation and interface tilt along sound, are in good agreement with observations. It is important to keep in mind that the control condition was dominated by the upper layer flow due to the deep lower layer except near the island. However, it should be noted that the small island near station A might have more effects on hydraulic characteristics on the sound than those discussed above. For further

understanding, more observations near the small island are required. There are also a number of complications that have not included into our discussions, for example, additional geometrical factors, frictional effects, the uneven bottom topography of the ice cover and even the convergence or divergence of the flow.

Chapter 4.Solitary Waves

4.1 Introduction

Over the past four decades, there have been many studies on the general nature of stratified flow over topography, through a constriction and related generation of internal waves. Most of these studies have been theoretical and utilized linear perturbation equations. In general, the linearized equations of motion do an adequate job in explaining internal wave propagation in the open ocean. However, when the amplitude of the internal wave is large in comparison with the characteristic depth of the ocean, nonlinear effects cannot be ignored. These nonlinear flows can be analyzed by solving the nonlinear equations. This will now be discussed.

Solitary waves, so called because they often occur as a single entity and are localised, include both nonlinear and dispersive effects. They are often found at the front of a depression or an elevation apparently steepening due to nonlinear effects. The nonlinearity can arise from interaction between tidal current and topography and/or constriction. This phenomenon has been observed in many areas, for example: in Massachusetts Bay (Haury et al,1979), Knight Inlet.(Farmer and Smith, 1980), Puget Sound (Geyer and Cannon, 1982), Observatory Inlet (Farmer and Freeland,1983), the Scotian Shelf (Sandstrom and Elliott,1984) and on Australia North West Shelf (Holloway, 1987). All of these have shown the existence of high-frequency internal wave trains instead of sinusoidal waves of tidal frequency around the sill, or continental slope where tidal flow is strongest. Based on observations and existing theory, the generation mechanism for internal solitary waves above a sill has been discussed by many authors. Maxworthy (1979), for example, through a series of laboratory experiments, found that periodic flow over an obstacle can be hydraulically critical, causing a depression downstream in the isotherms. After the tidal flow weakens and turns, the depression moved upstream evolving into a packet of solitary waves. Sandstrom and Elliott (1984) found that at

the shelf break of the Scotian Shelf off Nova Scotia, the pycnocline was depressed during the ebb tide. Following the ebb, the depression propagated upstream and evolved into solitary waves. The energy of the solitary waves came from the energy emitted by the modified internal tide. According to their data, the internal tide energy in the shelf zone was transferred with losses into the internal solitons, rather than into continuous low-amplitude internal waves. Thus, the universal internal wave spectrum of Garrett and Munk (1979) appears to be inadequate in describing the properties of the solitary waves (Wunch, 1975). In fact, the solitary waves can be studied in terms of the KdV type equation.

4.2 KdV Equation

Although the first solitary wave phenomenon was discussed by Scott Russell in 1844, the theoretical confirmation of Scott Russell's work had to wait until 1895 when two Dutch scientists, Kortweg and de Vries, derived their now famous KdV equation for the propagation of a wave in one direction on the surface of a shallow canal.The form of the KdV equation is

$$A_t+C_0A_x+\mu AA_x+\delta A_{xxx}=0 \qquad (4.1)$$

In equation (4.1), the subscript denotes differentiation, with time t and horizontal position x. C_0 is a linear long wave speed. The vertical displacement amplitude is

$$\eta=aA(x,t)\phi(z) \qquad (4.2)$$

where "a" is the amplitude of the vertical displacement due to the solitary wave, and $\phi(z)$ is the modal function which will be defined subsequently. The third term in equation (4.1) is the nonlinear term, while the last term is the dispersive term. The coefficients in equation (4.1) will be discussed later.

From its definition, the solitary wave can be explained in terms of a balance between nonlinear and dispersive effects. As we know, for very long waves, the dispersive effects are weak; the propagation speed of a long disturbance depends on the amplitude of the disturbance. Typically, one side of the wave form steepens as the wave propagates. The wave eventually breaks unless this steepening is counteracted by effects which tend to smooth out the layer gradients. On the other hand, for small disturbances, the dispersive effects dominate and the propagation speed essentially depends upon the wavelength. These waves tend to spread out as they propagate. Solitary waves, which retain their shape and speed, can be thought of as a special case in which the nonlinear steepening effects are exactly balanced by the dispersive effects. The existence of the balance implies a definite relationship between the speed, amplitude, and wavelength of the wave form. As an approximation, we can also use the KdV equation to describe a solitary wave-like disturbance. Since the dispersive effects vary with the depth of the medium, the existing analyses can be divided into three basic groups: shallow water, finite depth, and deep-water theory. In regard to modelling of nonlinear internal waves for the case of a straight-crest (one dimension), the Benjamin-Ono equation, the Kubota, or the Kortweg-de Vries(KdV) equation apply according to whether the wavelength is much smaller, of the same order or much larger than total water depth, respectively. The Benjamin-Ono equation requires the wave to be longer relative to an internal characteristic length scale of the thermocline region ($L/h \gg 1$) rather than the total fluid depth. These three limiting cases can be summarized as following, according to Koop and Butler(1981):

(i) Shallow-water theory

$$\lambda/H \gg 1 \quad h/H \leq O(1) \tag{4.3}$$

(ii)Deep water theory

$$\lambda/H \to 0, \quad \lambda/h \gg 1 \tag{4.4}$$

(iii)Finite-depth theory

$$\lambda/h \gg 1, \quad h/H \ll 1 \tag{4.5}$$

where λ, H and h are wavelength, water depth, and intrinsic scale of the

stratification (e.g. the depth of pycnocline), respectively.

Maxworthy (1978,1979) found that the whole spectrum of the KdV equation allowed the evolution of a train of solitary waves from an initial pulse. He concluded that the KdV equation could be used to crudely model events for a deep ocean. Segur and Hammack(1981) and Koop and Butler(1981) based on their experimental data found that the finite-depth model (Kubota, et al, 1978) predicted the data accurately only in so far as it agreed with the KdV equation. KdV predicted the solitary waves with remarkable accuracy, much better than the finite-depth theory even though the condition limit was satisfied with the finite-depth model. These results can be summarized as follows:

1)The KdV equation seems to have a relatively large range of validity, and has practical predictive value even when its assumptions are satisfied marginally.
2)For deep-water theory, using the theoretical KdV scale relationship, the wave length L is predicted to be "long" relative to the total depth, H (let $L/H \gg 10$) when $\varepsilon=a/h$ (i.e amplitude of wave /intrinsic length of density stratification) is smaller than about 0.001.
3)The finite-depth theory by itself has such a small range of validity that it has been difficult to find it experimentally.

Until now, most oceanographers used the KdV to explain observational data. For example, Osborne and Burch (1980) and Pierini (1989) have applied the KdV equation to understand internal wave fields in the Andaman sea and the Alboran Sea. They seem to behave like the KdV solution even though their observed wavelengths were comparable to the total water depth. Based on our observations, we will focus on the KdV equation (note, KdV refers to the first order one dimensional KdV).

Despite the relative depth limitation, the KdV equation can include shear, topography, variable cross-section, two-dimensions, viscous effects, and higher-order effects. Although we will not consider all of these in our

study, they are included in a general discussion below. The higher order KdV will be used in later discussions.

We will see later in this chapter that differences in velocity shear affect the variation of the nonlinear and dispersive terms by different combinations of δ and μ in equation (4.1). It is generally acknowledged that the effects of shear on the internal waves can be divided into two categories (Liu et al, 1981), the so called "kinematic" and "dynamic" effects. Kinematic effects refer to the change in wave form and wave speed of the internal wave as a result of the shearing action of the background flow. Dynamic effects refer to the possible energy and momentum exchanges between the waves and the background flow, where the shear represents an additional energy source. It can be shown that a weakly nonlinear internal wave does not exchange energy and momentum with the background flow in the absence of critical levels, where the linear wave speed equals to background velocity or $C_0=U_0(z)$. Therefore, the effect of shear on the wave is a purely kinematic change in wave speed and waveform. When a critical level is present, for any value of Z, μ=0, the solitary wave vanishes. Further,if the critical layer is viscosity dominated, the energy exchange between wave and background flow occurs at the critical layer. At this time, wave energy is absorbed by the background flow near the critical level. For unstable flow, the energy flow can go either direction. When nonlinearity is the dominant mechanism in the critical layer, no exchange of energy occurs between the wave and background flow. The effect of shear on the internal wave is again kinematic. Most long internal waves in the ocean belong to this case because the nonlinear effects are so large that the effect of viscosity is almost completely overwhelmed by the nonlinearity of the wave. If viscosity is ignored, steady conditions are assumed and the background flow does not influence the wave energetically. Normal mode solutions can be found even in the presence of critical levels (Tung, 1981). Maslowe and Redekopp (1982) also discussed shear flow effects on internal waves and found that when nonlinearity and viscosity have same order, and nonlinearity is dominant in the critical-layer, the wave mode can exist. In Manitounuk Sound, we will

neglect the shear effect on the solitary wave since the solitary waves occur at a time of very small shear.

Although KdV models usually neglect viscous effects, they can be important for certain situations. One interesting question is how viscosity affects the soliton wavelength. In a qualitative sense, with sufficiently large dispersive terms in the governing equations, viscosity should be important only in that it slowly attenuates the amplitude. When viscosity acts to decrease the disturbance amplitude nonlinearly, the strength of the viscous and nonlinear terms eventually become of comparable order. Koop and Butler (1981) found viscous effects to be small except for very small waves where $\varepsilon(t)<0.02$. To test the importance of viscosity, we can also compare the inviscid and the viscid modes.

The above theories ignore both topographic effects in the direction transverse to the wave propagation, as well as the change of cross-section. Johnson (1973a, b) and Grimshaw (1977) derived a KdV equation including topographic and cross-sectional effects, respectively, which was expressed as variable-coefficient KdV type equations. According to the model results of Grimshaw (1977), a decrease in channel width can be as effective as nonlinear processes in increasing the amplitude of the wave.

In some locations the 2-D KdV equation needs to be considered although usually the 1-D KdV is adequate to describe the soliton in a channel. An example of the 2-D assumption can be found in the studies by Liu et al (1985) in Sulu Sea. The choice of which dimension KdV equation should be used depends on the geometry of the basins and wave generation region concerned (i.e.whether or not need to include the spreading effect of the wave).The 2-D KdV can be(Kadomlsev-Petuiashuili,1970) expressed as:

$$\partial/\partial t(\eta_t + C_0\eta_x + 2\eta_{xxx} + \beta\eta\eta_x) + c_0/2\eta_{yy} = 0 \qquad (4.6)$$

This is called the K-P equation and is used for waves travelling predominantly along X and whose spatial variation along y is small compared with X: $(L_y/L_x)<<1$

4.3 Generation of Internal Solitary Waves in Manitounuk Sound

We consider three sets of solitary wave packets from our observations. Time series plots of current, salinity and temperature for two of these three examples are given in fig.2.8.

Fig.2.8 and the expanded time series plots (fig.4.1), demonstrate clearly the presence of high frequency internal solitary-like waves in a bore at station B, 30 min. after the tide turned from flood to ebb. Significant density changes took place within a relatively small time interval. Fluctuations of both salinity and temperature were quite large for the leading wave. The maximal peak-trough amplitude, based on equation (1), is estimated at about 2-3 meters, which is about 0.5m less than the value from computed contours of constant salinity. Of course, in a continuously stratified fluid, the water movements are not limited to the range of amplitude but extend through the water above and below the pycnocline. From the top figure of fig.4.1, the water parcels dropped sharply across the strong salinity gradient layer to about 6m depth. In front of the solitary wave, the isohalines were compressed and formed a strong horizontal gradient. The period of the leading waves was about 3-6 minutes (Table 2).

The generation mechanism of these solitary waves was ascribed to the upstream propagation of a bore at the start of the ebb. This bore, characterized as a stepwise variation of the isohaline level, was generated during the flood tide downstream of the hydraulic control (discussed in chapter 3). During the upstream propagation of the bore, a packet of solitary waves evolved from the bore due to the accumulation of the nonlinear effects. In particular, nonlinearities increased rapidly at the narrowest section, as found by Grimshaw (1978) for his variable-coefficient KdV mode and Farmer's (1977) observations in Babine Lake. The mechanism for soliton generation was similar to that discussed by Farmer and Smith (1980) and Maxworthy (1979), although their results were based on flow over a sill instead of through a constriction. Our data show that the transition of the bore appeared very much like the decomposition of a stepwise perturbation into a sequence of solitons. This is quite similar to the observation of a bore in the Caspian Sea by

TABLE 2

Series number	Date	Time	Period(min)	Amplitude(m)
1	21 April	09:48 --- 10:36	3.2	1.2
2	23 April	10:50 --- 11:26	5.1	2.1
3	24 April	11:18 --- 12:24	6.0	1.9
4	24 April	23:26 --- 0:28	4.0	2.2
5	25 April	11:40 --- 12:01	4.6	2.2
6	26 April	00:02 --- 00:38	3.0	1.8
Mean value			4.2	1.9

Table 2. Observed solitary wave,period and amplitude.

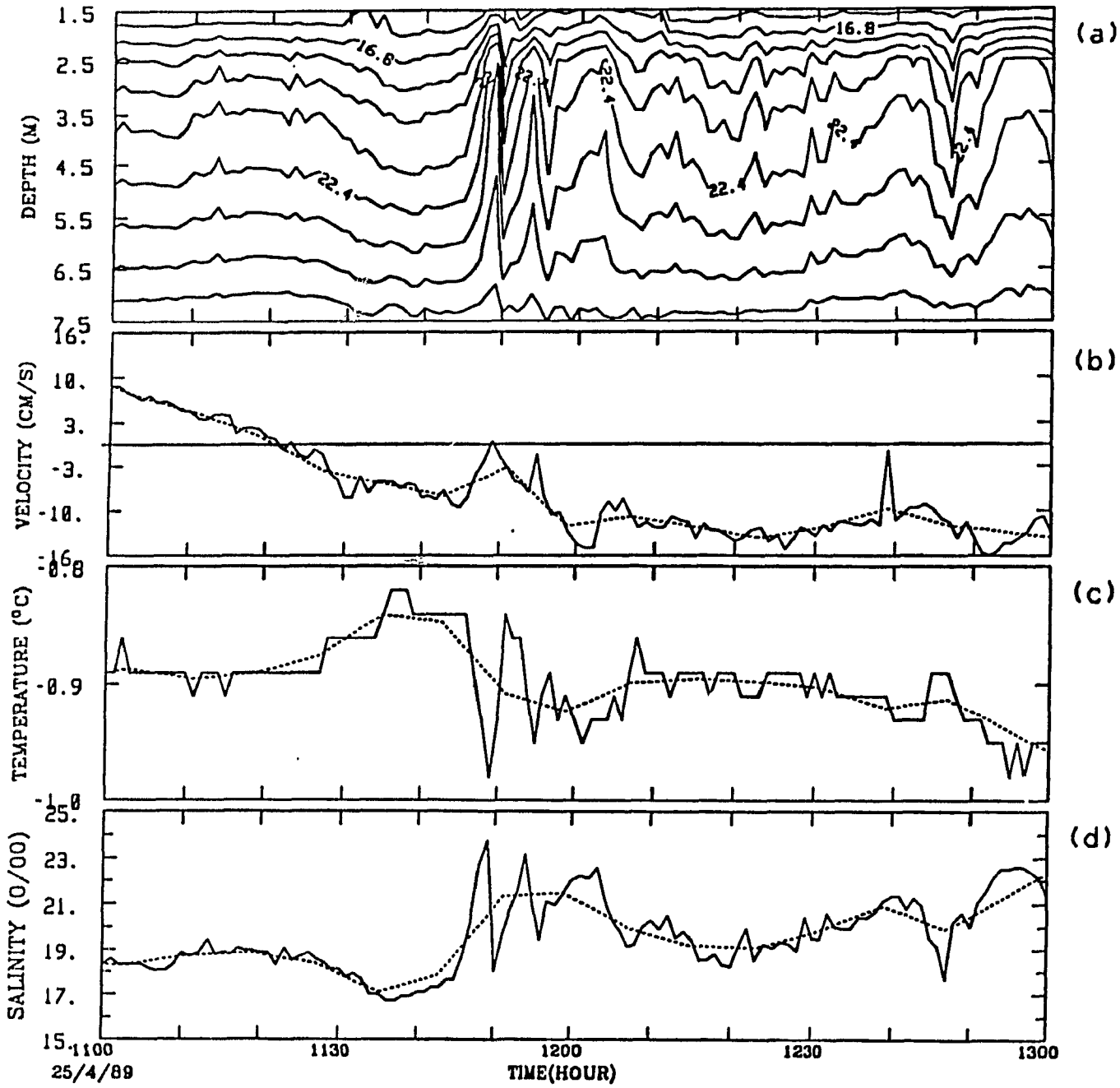

Figure 4.1. Expanded time series plots of salinity fluctuations at station B on April 25,1989. a: computed contours of constant salinity based on an interpolation of observations at discrete depths. The other three (b,c,d) were data at 2.5m of station B. The dashed line is the low pass filtered data set for each series.

Ivanov and Konyaev (1971), and the laboratory results of Baines (1984), both of whom showed internal solitons generated from the bore front. The numerical simulation of the decomposition of a smoothed "step" into solitons has been studied by Lee and Beardsley (1974). It must be noted that the wave in the sound represented a depression of the streamline, as expected for the stratification structure in the sound, i.e. μ in equation (4.1) is negative.

From station B data, the soliton was decomposed from a stepwise variation of the isohaline level. The procedure is illustrated in figs.4.1 and 4.2. In the dashed line of fig.4.1, the high frequency solitary waves were smoothed out, although the salinity bore (or temperature drop) can be seen in low pass data. The corresponding velocity signal would take either jump or drop depending on the velocity at the upper layer, because the wave was a depression wave. It should be noted that the bore (or drop) was larger than the filtered values shown in the dashed line of fig.4.1. Schematic showing how a localized initial wave form or bore $\eta(x,0)$ evolved into a group of solitons is presented in fig.4.2. Following the solitary waves, there was evidence of some other nonlinear events (bores, surges) which originated near station C. Although the available data extended over 2-3 weeks, solitary waves occurred only during the spring tide period, at the beginning of ebb. As shown in fig.2.3, spring tides began on 21 April, reached their peak on the 23rd and 24th, then started to decrease on the 26th. The corresponding solitary wave generation occurred during this period probably because of the weakened stratification of the water column. This suggests that more of the available energy has been extracted from the barotropic tide during the spring tide than during the neap. As discussed in chapter 3, the stronger flow during the spring tide will result in supercritical flow and a stronger bore. This, in turn, would provide more energy available for transfer into solitons. Since $Ri^{\#}$ is large at station B during the generation of solitary waves (see next chapter), the wave could not be generated by instability. The findings above agree with the discussion of the bore generation mechanism in the last chapter.

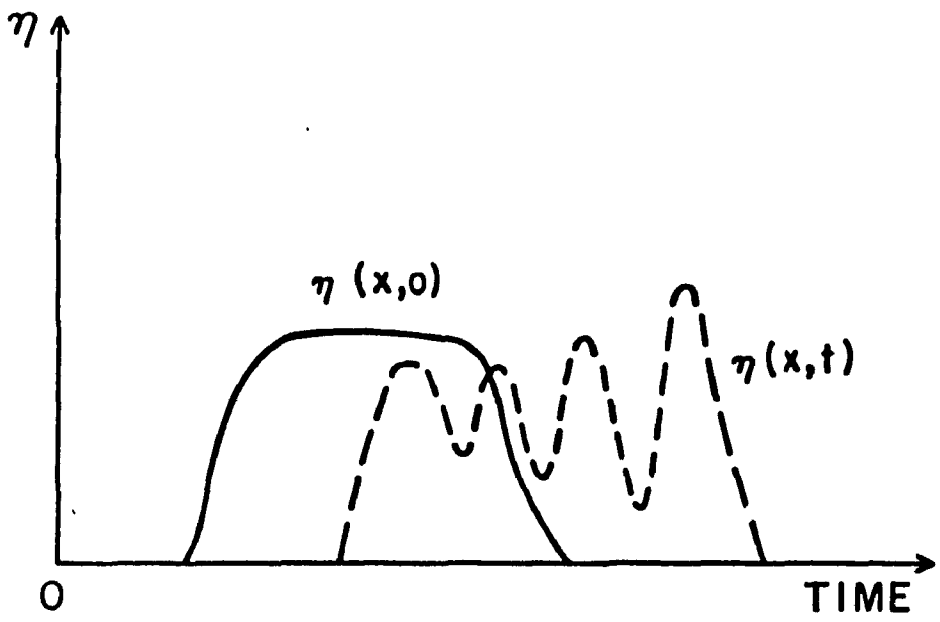

Figure 4.2. Schematic showing how a initial wave form (bore) can evolve into a group of solitary waves. Solid line refers to initial wave form.

4.4 Theoretical Model for Internal Solitary Waves

As mentioned before, different wavelength/depth ratios have their own type of KdV equation. By referring to the density profile (station B) observed on 29 April (fig.2.2), and considering both the stronger mixing due to the spring tide and the deeper pycnocline in the presence of solitary waves (see Chapter 2), the interface depth was estimated at about 3m. A linear wave phase speed of 0.54m/s can be estimated using the two-layer internal long wave theory. Since the observed wave period is about 3 to 6 min, the shortest horizontal scale of the wave must be of order 97 to 194m. Thus, the wave appeared to be long with respect to the total depth. At the same time, we have $h/H<\lambda$ (H=44m), so that the shallow water approximation and hence the KdV equation is valid in our case.

The surface solitary wave in shallow water can be characterized by the solution of the KdV equation. The theory was extended to internal solitary waves in shallow water by Benjamin(1966). One difference from surface wave theory is that an initial internal isopycnal elevation or a depression may become an internal solitary wave corresponding to different basic density structures, whereas only an initial free surface elevation can develop into a surface solitary wave. For internal waves, the basic density stratification may change the sign of the coefficient of the nonlinear term but the form of the KdV equation remains identical to the surface wave equation. In terms of the undisturbed density distribution, $\rho(z)$ and the stream function perturbation, Benny's (1966) analysis yielded a KdV type equation of first order in amplitude, similar to equation (4.1). Its solution has the form of the $Sech^2$ function. The modal function describes linear internal waves in the presence of mean shear $U_0(z)$. The solution to the eigenvalue problem (Grimshaw, 1982) is:

$$(\rho_0(C_0-U_0)^2\phi_z)_z+\rho_0N^2\phi=0 \qquad \text{for } 0<z<h \qquad (4.7)$$

$$\phi=0 \qquad \text{for } z=0 \qquad (4.8)$$

$$\phi=p\sigma(C_0-U_0)^2\phi_z \qquad \text{for } z=h \qquad (4.9)$$

where z=h is the free surface equilibrium position (see fig.4.3). $\rho_0(z)$ is the density and $N^2(z)=(-g/\rho_0)(\partial\rho_0/\partial z)=-(\sigma\rho_0)^{-1}\rho_{0z}$ is the Brunt-Vaisala frequency. Here, σ is small in the Boussinesq approximation. The number p is 0 or 1 according to whether the upper boundary is rigid or free and is equal to zero in the ice covered sound. The coordinate system is shown in fig.4.3. The linear wave phase speed C_0 is obtained from equation (4.7), and the coefficients in KdV are given by

$$\mu=3/2\left(\int_0^H\rho_0(C_0-U_0)^2\phi_z^3dz\right)/\left(\int_0^H\rho_0(C_0-U_0)\phi_z^2dz\right) \qquad (4.10)$$

$$\delta=1/2\left(\int_0^H\rho_0(C_0-U_0)^2\phi^2dz\right)/\left(\int_0^H\rho_0(C_0-U_0)\phi_z^2dz\right) \qquad (4.11)$$

where $C=C_0+\epsilon^2C_1$, $\epsilon=H/\lambda$, $C_1=(1/3)\mu a$, $\lambda^2a=12\delta/\mu$, and the solution for KdV is $A(x-ct)=a\mathrm{Sech}^2(x-ct)$. The situation for a critical level has been discussed at the beginning of this section.

We first approximate the density profile, for simplicity, as a two-layer model. The solitary wave solution, with upper and lower depth h_1 and h_2 and density ρ_1 and ρ_2 are (Osborne and Burch, 1980),

$$C_0=(g'h_1h_2/H)^{1/2} \qquad (4.12)$$

$$\mu=3C_0(h_2-h_1)/2h_2h_1 \qquad (4.13)$$

$$\delta=C_0h_1h_2/6 \qquad (4.14)$$

$$C=C_0-a\mu/3 \qquad (4.15)$$

and

$$\lambda=(-12\delta/a\mu)^{1/2} \qquad (4.16)$$

By using the values in Tables 2 and 3, Table 4 shows the parameter values associated with both first and second order KdV for a two layer fluid (Gear and Grimshaw, 1982). In order to compare the model with observation, wavelength is defined by the point at which the displacement has dropped to 10% of the maximum, or $\lambda=3.6L$, as Holloway (1987) suggested. The observed wave

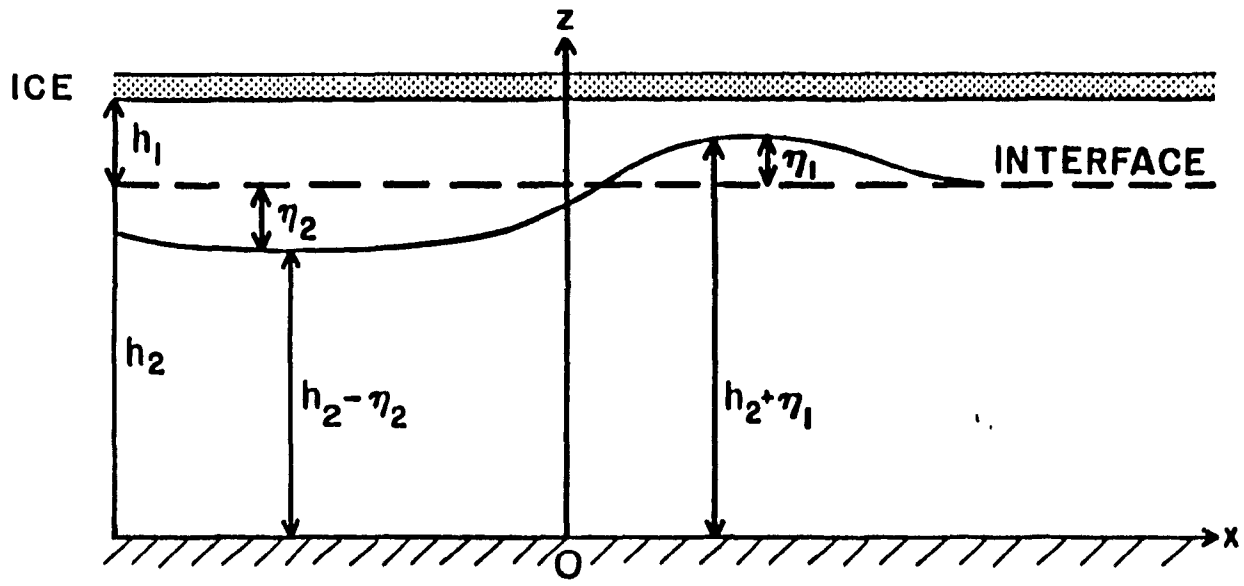

Figure 4.3. The coordinate system for KdV.

periods were estimated from the salinity oscillation corresponding to the definition of wavelength.

In Table 4, C/C_0 is about 1.2 so that the nonlinear correction to the linear phase was large. Another fact is that the calculated wave periods do not agree well with observations for the first order model. Actually, when the term of order $\varepsilon=a/h_1$= amplitude/thermocline thickness was large, the assumption of weak nonlinearity in deriving KdV may no longer be valid. Based on experimental results in a two-layer fluid, Koop and Butler (1981) concluded that the first order theory was valid for the wave amplitude as large as $\varepsilon=a/h_1=0.2$. The inclusion of second order nonlinear terms extends the useful range of the KdV theory to wave amplitudes of $\varepsilon=0.8$. Segur and Hammack (1982) argued that higher-order correction depended on h_2/h_1 and $(\rho_2-\rho_1)/\rho_1$. Later, Kao (1985) found that parameter a/H should be used. In our case, ε were 0.7, 0.6 and 0.6 for the three leading waves, respectively, as shown in Table 3. Therefore, it is necessary to have a second-order term correction in the KdV. The results show that the 2nd order correction is significant as seen in Table 4. For the second-order KdV, the correction to phase speed is nearly the same size as the first-order correction but opposite, according to the results of Sandstrom et al (1984) and Holloway (1988). Hence the second-order phase speed was approximately the same as the linear phase speed. When the second-order nonlinear term is included, the two-layer model is quite adequate to describe solitary waves in the sound.

To further understand the solitary waves and the relationship between the density structure and wave solutions, internal waves at the pycnocline of a continuously stratified fluid are examined.

A hyperbolic-tangent density profile is used to approximate the continuously stratified case (Kao,1985):

$$\rho(z)=\rho_0(1-\omega\mathrm{Tanh}\alpha(z-h_2)) \qquad (4.17)$$

where $\rho_0=0.5(\rho_1+\rho_2)$, $\omega=(\rho_2-\rho_1)/2\rho_0$, z is the vertical coordinate (like fig.4.3), and α^{-1} is a representive half-depth of the pycnocline thickness (fig.4.4). By solving equations (4.7), (4.8) and (4.9), we can find the solution for the

TABLE 3

Series number	h_1	h_2	ρ_1	ρ_2	ε
4	3.0	40.5	1010.66	1022.04	0.7
5	3.0	40.5	1011.3	1022.36	0.7
6	3.0	40.5	1012.76	1022.07	0.6

Table 3. The layer depth ,density and parameter $\varepsilon(a/h_1)$ for three series

TABLE 4

Series Number		Two-layer Model	
		1st-order	2nd-order
4	C_0	0.55	
	C	0.74	0.55
	λ	56	118
	t	1.3	3.5
	Δt	2.7	0.5
5	C_0	0.59	
	C	0.79	0.59
	λ	56	118
	t	1.2	3.3
	Δt	3.4	1.3
6	C_0	0.50	
	C	0.64	0.50
	λ	62	117
	t	1.6	3.9
	Δt	1.4	-0.9

Table 4. The long wave speed C_0(m/s),solitary wave speed C(m/s), wavelengthλ(m),period t(min) for first and second order two-layer model. Δt is the difference between the observed and model value.

modal function $\phi(z)$. This eigenvalue problem is solved numerically in a normalized coordinate with Z=0 at the bottom and Z=44m at the top. According to Kao(1985), the lowest eigenfunction mode has a maximum phase speed at the interface and corresponds to the interfacial internal wave, while the next mode corresponds to the "bulge-type" wave. It is shown that the higher order modes have phase speeds much smaller than the speed of the leading wave. In our case, the second mode speed in group 4 of Table 2 is 0.4m/s less than that for the first mode and does not satisfy our observations. For comparison, the second mode eigenfunction on April 24 (group 4) is also presented in fig.4.5. The eigenfunction for groups 5 and 6 are similar to group 4. With zero-order eigenfunction $\phi(z)$, the μ and δ in equation (4.10) and (4.11), and hence C and λ of the solitary wave, can be solved.

Using the values in Table 2 and 3, Table 5 presents the corresponding parameter values of the solitary waves, both for the $\rho(z)$ profile on 29 April (neap tide) and two hyperbolic-tangent density profiles for each solitary wave group. Two different density profiles used in the model for group 4 and profile on 29 April are plotted in fig.4.6. The density profiles for group 5 and 6 used in model were quite similar with that for group 4.

The results in Table 5 compare reasonably well with our measurements. In particular, we only use the first-order term in the KdV. This implies that its two-layer approximation may neglect some real-fluid effects in this nonlinear case. The Δt (the difference of observed and calculated period) in soliton group 4 and 5 is generally small. Δt in group 6 is quite larger when h_1=3m and α^{-1}=1.5m than when h_1=2m and α^{-1}=1.0m. This implies that the pycnocline might be thinner and shallower (i.e. small α^{-1} and h_1). In fact, the soliton group 6 occurred just after the largest spring tide. Its tidal amplitude was about 0.3m smaller than the peak value. Therefore, the relatively smaller shear and hence weak mixing might have caused a shallower pycnocline. The large Δt in group 7 of Table 5 also indicates that there was a difference in density profiles between spring and average tides. During spring tides, the stratification may have been weakened due to mixing.

TABLE 5

Series number		h_1=3m h_2=40m α^{-1}=1.5m	h_1=2.0m h_2=41.0m α^{-1}=1.0m
4	C_0	0.60	0.54
	C	0.63	0.59
	λ	143	90
	t	3.9	2.6
	Δt	0.1	1.4
5	C_0	0.57	0.51
	C	0.60	0.55
	λ	132	97
	t	3.7	2.9
	Δt	0.9	1.7
6	C_0	0.53	0.47
	C	0.55	0.50
	λ	158	100
	t	4.8	3.3
	Δt	1.8	0.9
7	C_0		0.39
	C		0.39
	λ		474
	t		20.2
	Δt		$\Delta t>10$

Table 5. The linear wave speed C_0(m/s),solitary wave speed C(m/s),wavelength λ(m) and period t(min) from the continuous stratification model. Δt is same as the Table 4. The series 7 is based on the density profile on 29 April

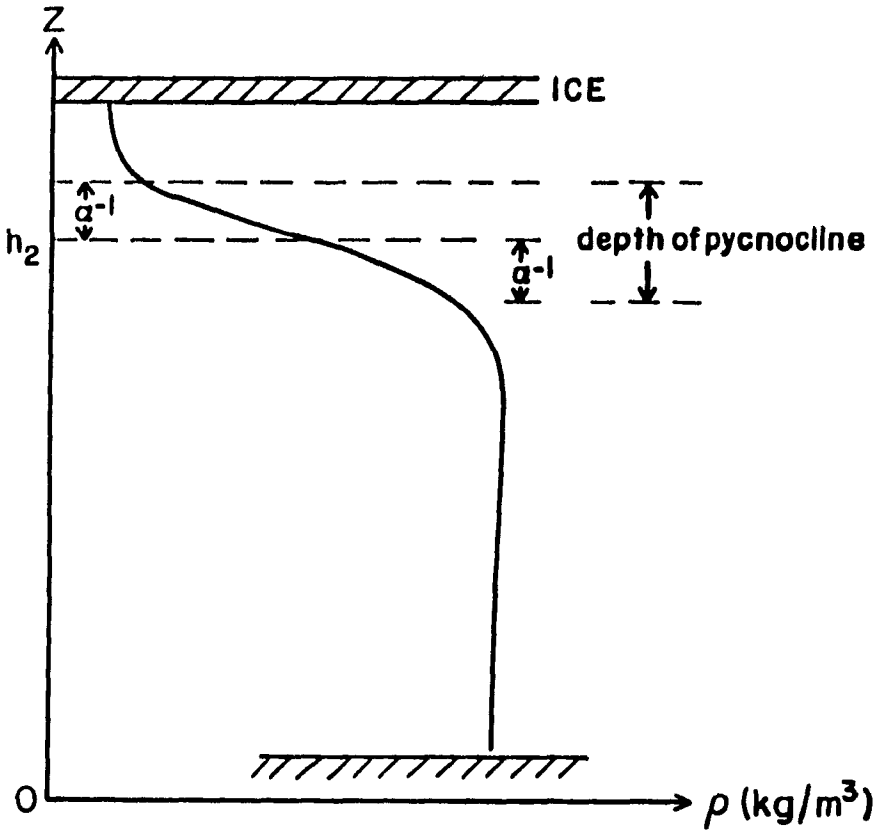

Figure 4.4. Typical hyperbolic-tangent density profile

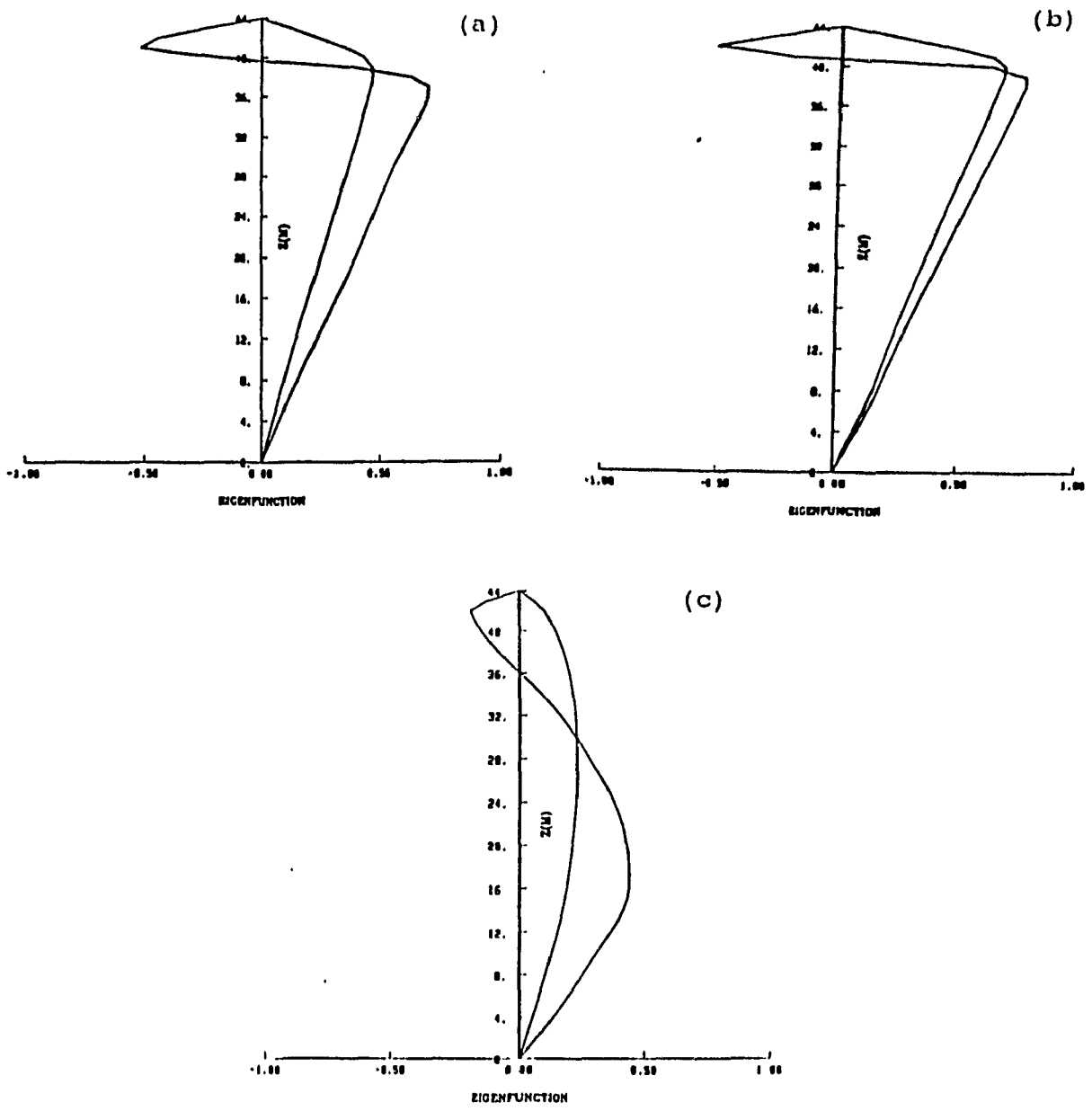

Figure 4.5. Shape of eigenfunction $\phi(z)$ for (a) h_1=3m, α^{-1}=1.5m on April 24,1989, (b) for h_1=2.0m, α^{-1}=1m, (c) for density profile on April 29.

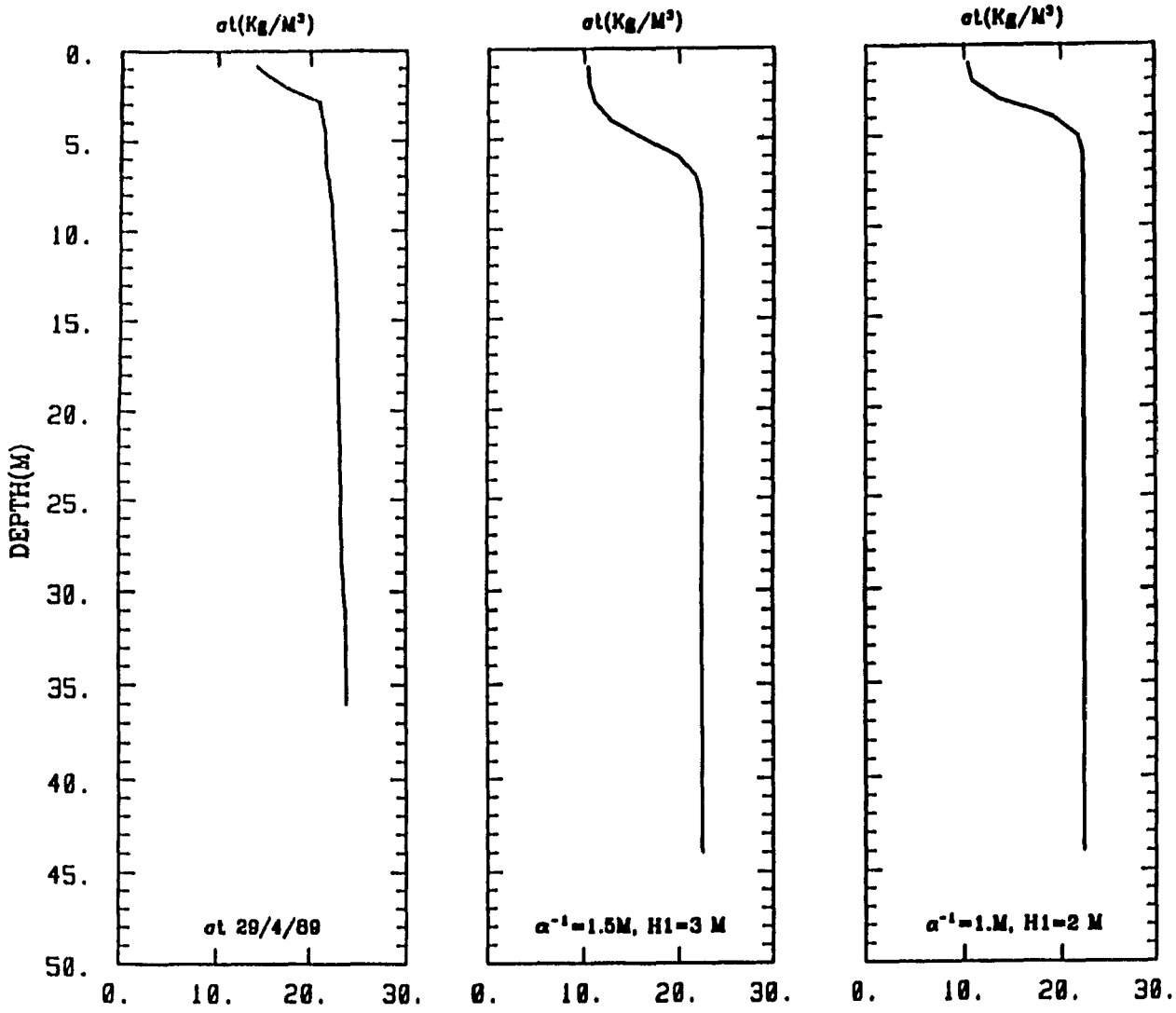

Figure 4.6. Three of typical density profiles, one from density profile on April 29, 1989. Two of them from hyperbolic-tangent density profile with different α^{-1} and h_1, and used for group 4 of solitary waves.

The results above suggests that α=0 in equation (4.17) may not be appropriate in our case. The results also agree with the Kao (1985), who found that the quantitative results of continuously stratified model were substantially different from those of the two-layer model for all important wave parameters. Indeed, the critical value of ε over which the second order nonlinear term must be considered seems to be larger for the continuous stratification model than for the two-layer in the Kao results. By comparing several models used in Tables 4 and 5, one finds that both the continuous density model and the second-order two-layer underpredict the wave period. The continuous density model has a larger phase speed and a longer wavelength than the two-layer model. However, all of them agree quite well with observations. Further studies with KdV based on the different density assumption are necessary.

Average parameter values in the sound for the two models are summarized in Table 6.

Since the phase speed of a solitary wave was larger than the general background flow speed, the waves will be continuously propagated upstream of station B, as mentioned before. Since the wave speed is proportional to the amplitude (equation 4.15), the leading wave with the largest amplitude travels the fastest. The second soliton had the second largest amplitude, and so on. The waves gradually separate from each other when they propagate further upstream because of their different speed. The absence of observations between stations B and C make it difficult to determine whether the solitary wave was generated between stations B and C, or only at station B when bore passed the narrowest section of the sound. To address this problem, a time dependent KdV model, with the bore as an initial condition, needs to be used. However, the propagation speed of bore from station C to B can be estimated as 0.4m/s, which is close to the calculated solitary wave speed. In other words, the propagation of a bore is also governed by nonlinear effects. Note, we have already taken into account the effects of background flow.

TABLE 6

No.	C(m/s)	λ(m)	t(min)
4	0.55	156	4.75
5	0.54	152	4.65
6	0.54	137	4.60
Mean value	0.53	148	4.67

Table 6. The average values of wave speed C, wavelength λ and period t from three models for No.4, 5, and 6 series.

TABLE 7

$\kappa(m^2/s)$	10^{-1}	10^{-2}	10^{-3}	10^{-4}
Length Scale(km)	0.7	2.0	7.0	20

Table 7. The eddy viscosity (κ) and the energy loss length scale.

4.5 Dissipation of Solitons

In order to obtain the length scale of the solitary wave energy loss, we use a model developed by Leone et al (1982), which was based on Keulegan's (1948) formulation of viscous decay of long linear surface waves. The model allowed a slow decay of an internal KdV soliton as it propagated over a long distance.

To use their model in the ocean, kinematic viscosity must be replaced by an eddy viscosity with a range of κ between 10^{-1}-10^{-4} m^2/s. The corresponding length scale for the wave energy is shown in Table 7.

For κ values between 10^{-1} and 10^{-2} m^2/s, decay length scales of 0.7 and 2.0km were obtained. They seem reasonable for our case, since there was no solitary wave signal detectable at station A. This implies that the wave was dissipated between stations A and B. However, the hypothesis above may not be accurate because it assumes that the internal wave propagated in a quiescent fluid. This is not satisfied in the sound. On the other hand, when a solitary wave moves into a moving fluid, wave breaking may happen before it can be completely dissipated. The breaking could occur because when the tide turns to flood and increases in strength, the wave may be unable to travel upstream against the stronger flood current.

Chapter 5.Mixing in the sound

5.1 Description

As discussed in chapter 2, salinity generally increased from station A to C at the 1.5m level and from station B to C at the other observation depths. Horizontal advection of higher salinity water from outside of the sound which could cause these salinity distributions along the sound was assumed negligble. In this chapter, the following mechanisms, which might contribute to the salinity regime along the sound, will be considered.

1.Strong velocity shear at the narrowest section of the sound, could generate a Kelvin-Helmholtz shear instability;

2.Critical and supercritical flow during the flood may result in intense mixing regions which would be advected upstream when the tide turned to ebb.

3.Dissipation of the solitary waves and bores transferred their energy into mixing.

It should be noted that the possible upwelling or downwelling between station B and A or B and C due to the flow convergence and divergence might also affect the conditions in the sound. However, whether or not these effects existed and how they could influence flow in the sound will not be discussed in the present thesis.

5.2 Kelvin-Helmholtz Instability

In steady and laminar flow, stability can be measured in terms of the gradient Richardson number, Ri, defined by:

$$R_i = -\frac{g}{\rho}\frac{\frac{\partial \rho}{\partial z}}{(\frac{\partial u}{\partial z})^2} \qquad (5.1)$$

where u is the horizontal velocity, ρ the density, and z a vertical coordinate upwards. Miles (1961) showed that the condition for stable flow was Ri>1/4 in the presence of small disturbances. When Ri<1/4 at some level in the fluid, the flow is not necessarily unstable. However, many examples of simple shear flow (Miles, 1963) did become unstable for some disturbances whenever Ri<1/4. The unstable flow often occurs near the region in which $\partial^2 u/\partial^2 z$ changes sign.

An examination of Ri number variability at stations A, B and C over the a tidal cycle during spring tide is shown in fig.5.1. The Ri^* in (c) is averaged in every 3 min. to delete high frequency noise. Ri^* at station A was generally large and the fluid relatively stable. The smallest Ri^* at stations B and C were reached when the flow at the upper and lower layers had maximal velocity for both stations. The Richardson numbers were calculated from values at 2.5m and 7.5m and do not include the smaller scale features.

5.3 Effects of the Internal Bore on mixing

The bores which formed near stations B and C affected the mixing processes in the sound, because they deformed the basic flow and might have induced large velocity gradients locally. As a result, the Richardson number and the stability of the flow would be reduced drastically.

The possibility of mixing caused by an internal bore was examined by several authors. Gardner and Smith (1978) concluded that the mixing events in the Duwamish were caused by an internal hydraulic jump. However, the experiments of Lawrence (1985) and Rajaratnam & Subramanyan (1985) found that the primary cause of mixing was not the jump itself, but the supercritical shear layer formed upstream of the jump. The Ri number for the two-layer can be expressed as:

$$R_i = -g' \frac{h_1 + h_2}{(u_2 - u_1)^2} \qquad (5.2)$$

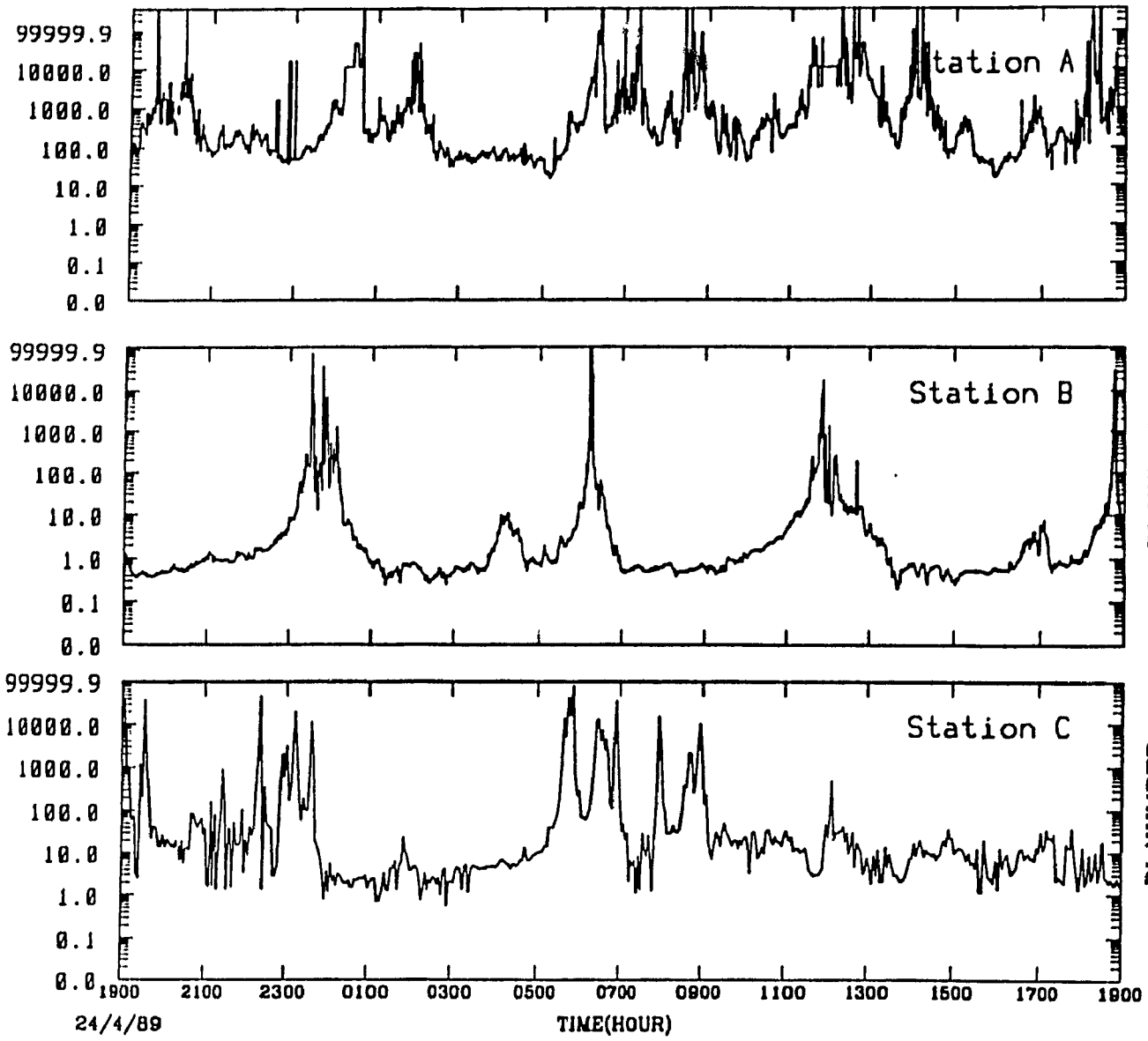

Figure 5.1.Time series of Richardson number for stations A, B and C. The vertical axis is 'log' scale.

According to the definition of composite Froude number G^2 (equation 3.2), theinternally subcritical flow is satisfied with the stable condition, or when $G^2<1$, $Ri>1/4$. Therefore, an instability is possible in the region with higher composite Froude number. In our case, the bores were formed near stations B and C when the flow was supercritical. The critical flow at station B occurred simultaneously with the lowest Ri number (figs.3.1 and 5.1) although there was only a trough of $Ri^{\#}$ for supercritical flow at station C. However, the lower $Ri^{\#}$ should be at upstream of station C, that is the upstream of the bores according to Lawrence (1985) and Rajaratnam & Subramanyan (1985). The increased separation of isohalines observed at stations B and C when bores, drops or supercritical flow existed (fig.2.13 (b) and (c)) also implies increased vertical mixing at these time. The dissipation of internal bores can also increase the potential energy of fluid. This is discussed in next section.

5.4 The Effects of Internal Solitons on mixing

Figs.2.10 and 2.11 showed that there was a salinity difference between stations B and A as well. At the 1.5m level, the salinity increased from station A to B (fig.2.11). However, the negative (S_B-S_A) during spring tides at the 2.5m level suggests that the saltier water source might exist between station B and A at this level and be advected to station A during the ebb. Comparing data of station A with station B, we can see that solitary-like waves and bores were dissipated between these two stations during each tidal cycle. We expect that part of the dissipated energy both from bores and solitary waves would increase the potential energy of the fluid. Adopting the method used by Sandstrom and Elliott (1983), the energy dissipation can be roughly estimated as follows: for a soliton, the total energy is calculated from $E_s=(4/3)g\Delta\rho a^2\lambda$. With a=2.2m, λ=131m and $\Delta\rho$=11.1 kgm^{-3} in our case, E_s was $1.3\chi10^5$J/m of crest length. According to the results of the previous chapter, the dissipation distance was about 2km over a time interval of about 3.5×10^3

s if we assume that the wave propagation speed was constant. Thus, the average rate of dissipation was typically 1.4×10^{-2} wm^{-2}. According to Osborn(1980), only 15-20% of energy per unit length would be transferred into an increase of potential energy of the water column, or about 2.8×10^{-3} Wm^{-2} in our case. If we choose the mixed layer of 3m, it can be shown an increase of mixed layer depth about 0.1m during the wave dissipation period according to $\Delta(PE)=1/2g'\rho h_1(\Delta h_1)$. It is obvious that if the dissipation distance was 0.7km (Table 7.), the increase of mixed layer depth would be larger than 0.1m. Note, we assume that the solitary waves were generated at the narrowest section and dissipated as it propagated towards station A during the ebb. Since a packet of solitons consisted of 4-5 single waves, the soliton energy available for increasing the potential energy of the water column would be larger. Similarly, based on Su's (1976) model and following Holloway (1989), the energy loss of an individual bore from the station C during flood to a region between A and B during the ebb was about 5×10^5 J/m. This seems quite close to the total energy of five solitary waves in the sound. We can therefore argue that the solitary waves and the following bores resulted in increased mixing as they dissipated between stations B and A.

It should be noted that vertical mixing was enhanced in the area where the solitary waves were observed according to the increased separation of isohalines in fig.2.13 (b). This saltier water will be advected upstream with the ebb.

From the above analysis, it suggests that the supercritical induced shear instability was the major cause for vertical mixing in the region between station B and C. In a quantitative sense, we can calculate the critical velocity shear by using the time-constant hyperbolic-tangent density profile similar to before.

$$\left(\frac{\partial U}{\partial Z}\right)_{critical}=\left(\frac{16g\alpha\varpi}{(1-\varpi\tanh\alpha z)\,(e^{\alpha z}+e^{-\alpha z})}\right)^{\frac{1}{2}} \qquad (5.3)$$

Substituting the parameters for lowest $Ri^{\#}$, the $(\partial u/\partial z)_{critical}$ is about 0.16 s^{-1} at the middle of the pycnocline. If $\partial u/\partial z<(\partial u/\partial z)_{critical}$, the flow is stable. On the other hand, the density gradient also influences the Ri number. The relationship between the velocity shear $\partial u/\partial z$ and density gradient $g\partial\rho/\rho\partial z$ is plotted as figs.5.2 and 5.3 for station B and C, respectively. Fig.5.2 shows that most of the Ri numbers ranged over $0.25<Ri<0.5$ with smaller Ri during the ebb. Most of the $\partial u/\partial z$ at this Ri range were larger than 0.1 s^{-1}, which agrees well with the critical value calculated from the hyperbolic-tangent density profile. Although the density gradient increased rapidly when $\partial u/\partial z>0.13$ s^{-1}, the stronger shear effect still dominated the Ri number and kept them below 0.5 during the ebb during which the bore was observed at station B. Most $Ri^{\#}$ values ranged between 1. and 0.5 during the flood, due to the weaker shear flow. At station C (fig.5.3), small $Ri^{\#}$ values occurred during both flood and ebb when the vertical density gradient was small. The $\partial u/\partial z$ there was smaller compared to station B, and hence $Ri^{\#}$ was larger.

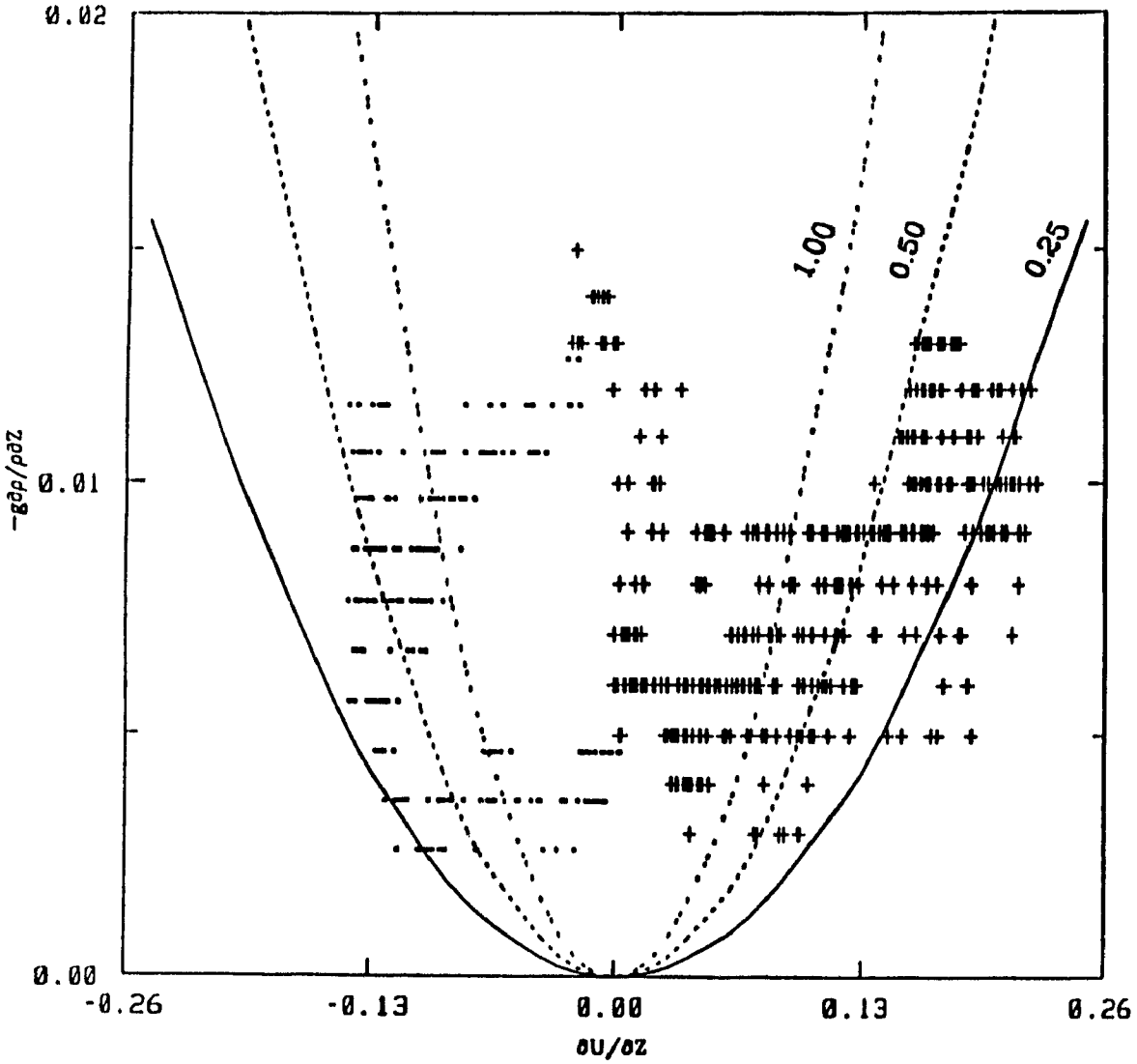

Figure 5.2.Ri number at station B in the velocity shear ($\partial u/\partial z$) and density gradient ($g\partial\rho/\rho\partial z$) plane. The sign '+' refers to the Ri number during the ebb; '-' refers to flood.

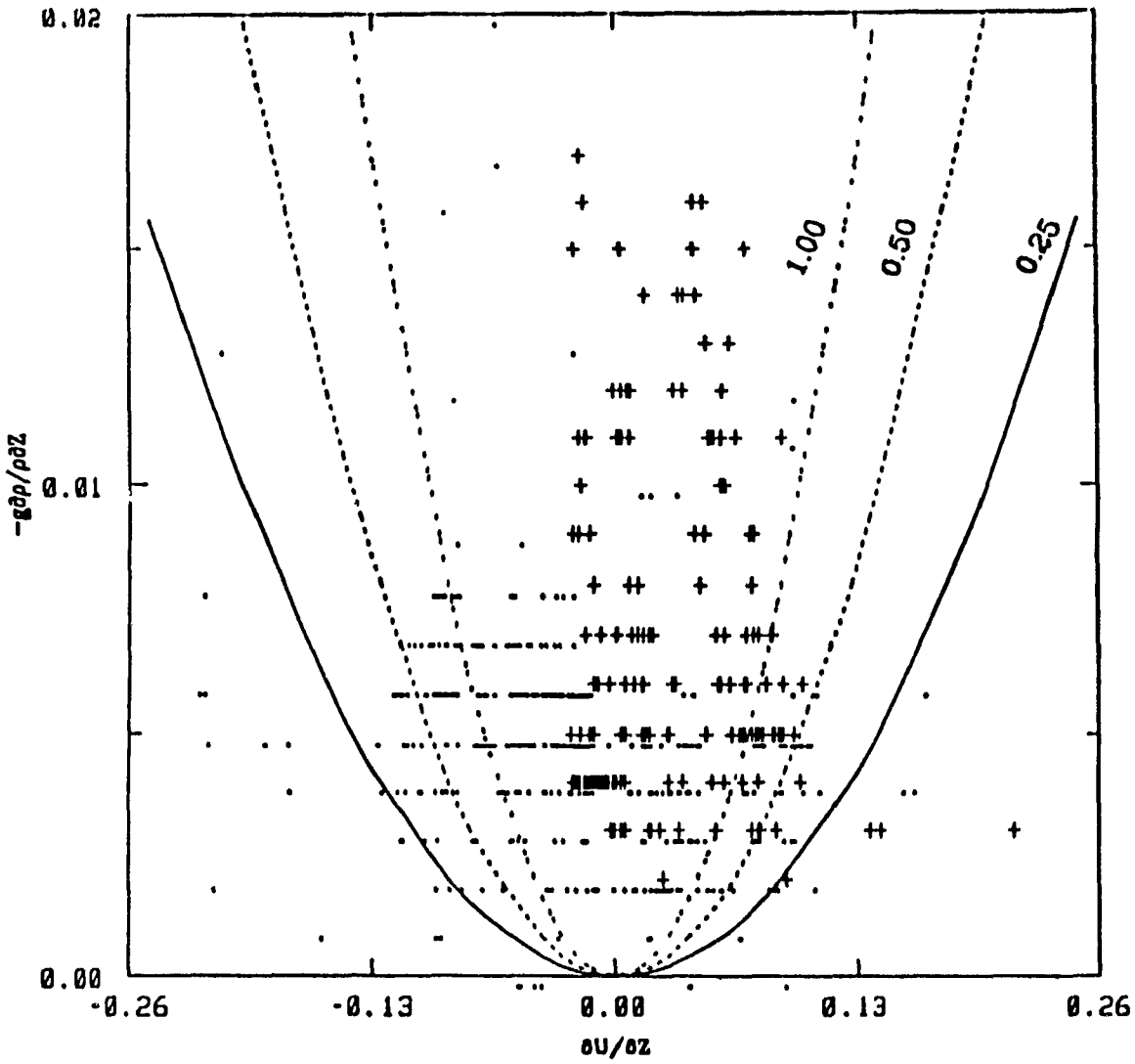

Figure 5.3. Ri number at station C in the velocity shear ($\partial u/\partial z$) and density gradient ($g\partial\rho/\rho\partial z$) plane. The sign '+' refers to the Ri number during the flood; '-'refers to ebb.

Chapter 6.Conclusions

Flow through a horizontal constriction in the sound during spring tides was studied based on the two-layer hydraulic theory. The observed asymmetry and rapid transition of the interface depth was explained in terms of the hydraulic characteristics of the flow.

It was shown that the sound was characterized by both maximal and submaximal exchange during the different tidal phase. The flow was subject to a critical transition at the narrowest section and downstream of the narrowest section. Internal hydraulic bores were generated when the flow returned to the subcritical state downstream of the supercritical region. The shallower region near a small island upstream had a sill like effect and resulted in a hydraulic drop.

The bores propagated upstream from the control station when the tide turned to ebb. High frequency internal solitary waves were generated near the narrowest section from the upstream propagating bores. The waves were described by the KdV equation. Comparisons of several KdV models in terms of different stratification approximations revealed that the continuous stratification model might be more suitable in explaining the nonlinear wave field. In this regard, it should be noted that the density profiles were not taken simultaneously with the arrival of the internal wave train. Therefore, further field work may be needed for more rigorous results.

The region of supercritical upper layer flow downstream of the control, the presence and dissipation of the solitary waves and bores were the major causes responsible for the along-channel salinity distribution over a semi-diurnal tidal cycle in the sound.

Since conditions in the sound are highly controlled by tidal force, the subjects about time dependent hydraulics, solitary waves and general circulation in the sound should be addressed in the future studies.

References

Armi,L., and D.M.,Farmer, 1985: The internal hydraulics of the Strait of Gibraltar and associated sills and narrows, Oceanologica.Acta 8:37-46.

----, 1986: The hydraulics of two flowing layers with different densities, J.Fluid Mech., 163:27-58.

----, and D.M.Farmer, 1986: Maximal two-layer exchange through a contraction with barotropic flow, J.Fluid Mech.164:27-51.

----, and D.M.Farmer, 1988: The flow of Mediterranean water through the strait of Gibraltar, Prog. Oceanogr., Vol.21, No.1 edited by V.A. Martin and R.L.Smith.

Baines,P.G., 1984: A unified description of two-layer flow over topography, J.Fluid.Mech., 146:127-167.

Benjamin,T.B., 1966: Internal waves of finite amplitude and permanent form, J.Fluid Mech., 25:241.

Benny,D.J., 1966: Long non-linear waves in fluid flows, J.Math Phys., 45:52-63,1966

Farmer,D.M and J.D Smith, 1978: Non-linear internal waves in a fjord. In J.C.J Nihoul(ed.) Hydrodynamics of Estuaries and Fjords. Elsevier, Amsterdam.

----, and R.A.Denton, 1985: Hydraulic control of flow over the sill in Observatory Inlet, J.Geophys.Res., 90:9051-9068.

----, 1978: Observation of long nonlinear internal waves in a lake, J.Phys.Oceanogr. 8(11):63-73.

----, and H.J.Freeland, 1983: The physical oceanography of fjords, Prog.Oceanogr. 12:147-220.

----, and L.Armi, 1986: Maximal two-layer exchange over a sill and through the combination of sill and contraction with barotropic flow, J.Fluid Mech. 164:53-76.

----, and L.Armi, 1988: The flow of Atlantic water through the strait

of Gibraltar, Prog. Oceanogr., Vol.21, No.1 edited by V.A. Martin and R.L.Smith.

Forberg,B,and G.B.Whitham, 1978: Numerical and theoretical study of certain non-linear wave phenomena, Philos.Trans.R.Soc. London Ser.A, 289:373-404.

Gardner,G.B.and J.D.Smith, 1978: Turbulent mixing in a salt wedge estuary. In Nihoul, J.C.J.ed Hydraulics of Estuaries and Fjords. Elsevier, 23:,79-106.

Gear J.A.and R.H.J.Grimshaw, 1983: Second-order theory for solitary waves in shallow fluid, Phys.Fluids, 26:14-29.

Grimshaw,R.H.J., 1978: Long nonlinear internal waves in channels of arbitrary cross-section, J.Fluid.Mech. 86:415-431.

----, Solitary waves in density stratified Fluids,in U.Nigel and J.Engelbrecht, Eds. Nonlinear Deformation Waves,Springer Verlag

Haury,L., G. Briscoe and M.Orr, 1979: Tidally generated internal wave packets in Massachusetts Bay,Nature, 278:312-317.

Holloway,P., 1987: Internal hydraulic jumps and solitons at a shelf break region on the Australian north west shelf, J.Geophys. Res., 92, 5405-5416.

----, and N.Smith, 1988: Hydraulic jump and undular bore formation on a shelf break, J.Phys.Oceanogr., 18.

Halpern D., 1969: Observation on short-period internal waves in Massachusetts Bay, Mass.Inst.of Technol.Cambridge Mass.

Ingram,R.G., 1983: Salt entrainment and mixing processes in an under-ice river plume. In Coastal Oceanography (Gade,H.G.ed), New York, Plenum Press,551-564.

----, J.C.Osler, and L.Legendre, 1989: Influence of internal wave induced vertical mixing on ice algal production in a highly stratified sound, Estuarine, Coastal and Shelf Science, 29:435-446.

Ivanov,V.A, and K.V.Konyaev, Bore on a thermocline,IZV.Akad,Nauk

SSSR Fiz.Atmos.Okeana 12(4), 416-423,1976 (IZV. Acad. Sci USSR Atmos.Oceanic Phys.,Engl Transl.,12(4),1976)

Johnson,R., 1972: Some numerical solutions of a variable-coefficient KdV equation J.Fluid.Mech. 54:81-91.

----, 1973b: On the development of a solitary wave moving over an uneven bottom,Proc. Camb. Phil. Soc, 73,183-203,1973,3) On an asymptotic of KdV equation with slowly varying coefficients, J.Fluid Mech. 60:813-824.

Kao,T.W,F.S.Pan, and D.Renouard, 1985: Internal solitons on the pycnocline: Generation, propagation, and shoaling and breaking over a slope, J.Fluid Mech.,159:19-53.

Koop,C., and G.Butler,G., 1981: An investigation of internal solitary waves in a two-fluid system, J.Fluid.Mech., 112:225-251.

Kubota,T., D.Ko, and D.Dobbs, Propagation of weakly non-linear internal wave in a stratified fluid of finite depth, A.I.A.A.J. Hydronauticals, 12:157-165.

Larouche.P, 1984: Mesures oceanographiques dans le panache de la Grande riviére de la Baleine, hiver 1983, Rapport statistique Canadien sur l'hydrographie et les science océaniques No. 20, Fisheries and Oceans Canada, Quebec, Canada, 706 p.

Lawrence G.A , 1985: The hydraulics and mixing of two-layer flow over an obstacle. Report UCB/HEL-85/02,University of California, Berkeley.

Lee,C. and Beardsley, 1974: The generation of long nonlinear internal waves in a weakly stratified shear flow, J. Geophys. Res , 79:453-462.

Leone,C, H.Segur and J.L.Hammack, 1982: Viscous decay of long internal solitary waves, Phys. Fluids 25(6)

Lewis,R.E. 1985: Intense mixing periods in an estuary. Turbulence and Diffusion in Stable Environments.In Hunt JCR(ed), Oxford, Press, New York, 315-319.

Liu,A. and D.Benney, 1981: The evolution of nonlinear wave trains in stratified shear flows Stud.in Appl.Math. 64:247-269.

----,J.R.Holbrook and J.R.Apel, 1985: Non-linear internal wave evolution in the Sulu Sea, J.Phys.Oceanogr., 15(2),1613-1624.

Long,R.R., 1953: Some aspects of the flow of stratified fluids.I.A theoretical investigation. Tellus 5:42-57.

----, 1955: Some aspects of the flow of stratified fluid III, continuous density gradients, Tellus,7:342-357.

----, 1965: On the Boussinesq approximation and its role in the theory of internal waves, Tellus,17:46-49.

----, 1974: Some experimental observations of upstream disturbances in a two-fluid system Tellus, 26:313-317.

----, 1975· The influence of shear on mixing across density interface, J.Fluid Mech. 70:305-320.

Maslowe,S.A and L.G.Redekopp, 1980: Long non-linear waves in stratified shear flows, J.Fluid Mech. 101,:21-348.

Maxworthy,T.A., 1979: Note on the internal solitary waves produced by tidal flow over a three-dimensional ridge, J.Geophys. Res., 84:338-346.

Mile,J.W., 1961: On the stability of heterogeneous shear flows, J.Fluid Mech. 10:496-508.

----, 1979: On the Kdv equation for a gradually varying channel, J.Fluid Mech. 91:181-190.

Mysak,L.A., 1984: Nonlinear Internal Waves, Hydrodynamics of Lakes: CISM Lecture, 129-152, edited by K.Hutter, Springer Verlag Wien-New York.

New,A.L., K.R.Dyer,K.R. and R.E.Lewis, 1987: Internal waves and intense mixing periods in a partially stratified estuary. Estuarine Coastal Shelf Sci.,24:15-33.

Osborne,A. and T.Burch, 1980: Internal solitons in the Andaman Sea, Science,208:451-460.

----, 1980: Estimates of the local rate of vertical diffusion from dissipation measurements. J.Phys.Oceanogr. 10:83-89.

Ostrovsky L.A and Yu.A.Stepanyants, 1989: Do Internal Solitons exist in the ocean? Reviews of Geophysics, 27:293-310.

Partch,E.N.and J.D.Smith, 1978: Time dependent mixing in a salt wedge estuary. Estuarine Coastal Shelf Sci. 6:3-19.

Pierini,S., 1989: A model for the Alboran Sea internal solitary waves, J.Phys.Oceanogr., 19:755-772.

Rajaratnam W.and S.Subramanyan, 1985: Plane turbulent buoyant surface jets and jumps, J.Hydraul.Res. 23:131-146.

Sandstrom,H. and J.Elliott, 1984: Internal tide and solitons on the Scotian Shelf: A nutrient pump at work, J.Geophys.Res., 89,6415-6426.

Sandstrom,H, J.Elliott, and N.Cochrance, 1989: Observing groups of solitary internal waves and turbulence with batfish and echo-sounder, J.Phys.Oceanogr,19:987-997.

Segur,H.,and J.Hammack, 1982: Soliton models of long internal waves, J.Fluid Mech.,118:285-304.

Stacey,M and L.Zedel, 1986: The Time-dependent hydraulic flow and dissipation over the sill of Observatory Inlet, J.Phys. Oceanogr., 16,1062-1076.

Stommel,H.and H.G.Farmer, 1952: Abrupt change in width in two-layer open channel flows.J.Mar.Res. 11,205-214.

Su,C.H., 1976: Hydraulic jump in an incompressible stratified fluid. J.Fluid Mech. 73:3-47.

Tung,K.,D.Ko,and J.Chang, 1981: Weakly nonlinear internal waves in shear, Stud.Appl.Math. 65:189-221.

Turner J.S., 1973: Buoyancy effects in fluids, Cambridge University Press, Cambridge.

Wood I.R. and J.E.Simpson, 1983: Jumps in layered miscible fluids. J.Fluid Mech., 149:,329-342.

Wunsch,C., 1975: Deep ocean internal waves: What do we really know? J.Geophy.Res., 80:339-343.